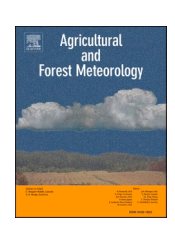
ELSEVIER

Contents lists available at ScienceDirect

#### Agricultural and Forest Meteorology

journal homepage: www.elsevier.com/locate/agrformet



## Magnitude and seasonal variation of $N_2O$ and $CH_4$ emissions over a mixed agriculture-urban region



Xin Tong <sup>a</sup>, Bert Scheeren <sup>a</sup>, Fred Bosveld <sup>c</sup>, Arjan Hensen <sup>d</sup>, Arnoud Frumau <sup>d</sup>, Harro A.J. Meijer <sup>a</sup>, Huilin Chen <sup>a,b,\*</sup>

- a Centre for Isotope Research (CIO), Energy and Sustainability Research Institute Groningen (ESRIG), University of Groningen, Groningen, the Netherlands
- b Joint International Research Laboratory of Atmospheric and Earth System Sciences, School of Atmospheric Sciences, Nanjing University, Nanjing, China
- Royal Netherlands Meteorological Institute (KNMI), De Bilt, the Netherlands
- <sup>d</sup> Netherlands Organisation for Applied Scientific Research (TNO), Petten, the Netherlands

#### ARTICLE INFO

# Keywords: Nitrous oxide (N<sub>2</sub>O) Methane (CH<sub>4</sub>) Emissions Seasonal variations Nighttime

#### ABSTRACT

Inventory estimates of N2O and CH4 emissions disregard temporal and spatial variabilities, which hinders the search for effective local strategies to lower greenhouse gas emissions. We have quantified the emissions of N2O and CH4 in a mixed agriculture-urban region using two independent approaches, i.e., the vertical gradient method (VGM) and the radon-tracer method (RTM), compared the estimated annual fluxes with the EDGARv6.0 emissions, revealed the seasonal variations of the VGM fluxes, and inferred the sources that most likely cause the seasonal variations based on the footprint analysis even though our methods cannot attribute different sources. We show that the annual RTM estimates represented by the mode of lognormal fit for N<sub>2</sub>O and CH<sub>4</sub> are 0.4 g m<sup>-2</sup> yr<sup>-1</sup> and 12 g  $m^{-2}$  yr<sup>-1</sup>, and the VGM estimates are  $0.6 \pm 0.3$  g  $m^{-2}$  yr<sup>-1</sup> and  $13 \pm 4$  g  $m^{-2}$  yr<sup>-1</sup>, respectively. Furthermore, the average EDGARv6.0 emissions constrained by the VGM and the RTM footprints are  $1.3 \text{ g m}^{-2}$  $yr^{-1}$  and  $0.9 \text{ g } m^{-2} yr^{-1}$  for  $N_2O$ , and  $21 \text{ g } m^{-2} yr^{-1}$  and  $18 \text{ g } m^{-2} yr^{-1}$  for  $CH_4$ . Compared to our estimated fluxes, EDGARv6.0 N<sub>2</sub>O and CH<sub>4</sub> emissions are both overestimated; for N<sub>2</sub>O, it is mainly caused by an overestimation of the chemical industry's emission. Moreover, in contrast to EDGARv6.0's nearly constant monthly emissions throughout the year, the VGM estimates of N2O and CH4 show seasonal variations with relatively high values from March to September, which is most likely caused by agricultural activities. Our study demonstrates that large nighttime vertical gradients of atmospheric N2O and CH4 mole fractions at a tall tower can be used to derive surface fluxes by the VGM; taken together with the RTM fluxes, both the annual means and the temporal variations of N2O and CH4 emissions can be constrained on a regional scale.

#### 1. Introduction

Nitrous oxide ( $N_2O$ ) and methane (CH<sub>4</sub>) are two potent greenhouse gasses, with a global 100-year warming potential of 265 and 28 times that of CO<sub>2</sub>, respectively (Myhre et al., 2013). Since preindustrial times, the atmospheric concentrations of  $N_2O$  and CH<sub>4</sub> have been steadily increasing due to anthropogenic emissions.  $N_2O$  and CH<sub>4</sub> emissions on regional to global scales can be estimated from inverse studies based on atmospheric concentration observations, the so-called "top-down" approach, or from inventory studies based on activity data and emission factors, the so-called "bottom-up" approach. For  $N_2O$  emissions, global estimates by the two approaches are broadly consistent (Huang et al., 2008; Tian et al., 2020) while for hot-spot regions they differ

significantly (Eckl et al., 2021; Fu et al., 2017; Huang et al., 2008; Jeong et al., 2012). For CH<sub>4</sub> emissions, a consensus is lacking for estimates on global to regional scales; several recent studies indicate that the larger bottom-up global emission estimates of CH<sub>4</sub> compared to the top-down results are mainly due to the larger estimates of the emissions from wetlands and inland water systems (Kirschke et al., 2013; Saunois et al., 2020). For certain regions, the two approaches also yield different estimates of emissions due to oil and gas supply chain and agriculture (Alvarez et al., 2018; Ganesan et al., 2015).

Variable techniques have been applied to provide independent top-down estimates of  $N_2O$  and  $CH_4$  emissions. At regional scales ( $\sim 10 \, \text{km}^2$  to  $\sim 10^6 \, \text{km}^2$ ) complementary techniques include eddy covariance (EC) measurements at tall towers (Haszpra et al., 2018), vertical

E-mail addresses: huilin.chen@rug.nl, huilin.chen@nju.edu.cn (H. Chen).

<sup>\*</sup> Corresponding author.

gradient estimates using tall tower observations (Desai et al., 2015; Griffis et al., 2013; Winderlich et al., 2014), the <sup>222</sup>Rn tracer method (Grossi et al., 2018; Van Der Laan et al., 2009), and the mass balance approach (Karion et al., 2015; Yacovitch et al., 2018). These approaches estimate the integrated surface emissions from all sources in a certain region, while avoiding the potential bias of transport models in top-down studies or the scale-up uncertainties in bottom-up studies.

In this paper, we investigate the characteristics of regional emissions of N2O and CH4 over a mixed agricultural-urban region in the Netherlands based on continuous concentration profile measurements at a tower of 213 m height. The N2O and CH4 emissions in the area surrounding the tower are from various sources and spatially variable. Within a ~ha scale area, intensively managed grassland on peat soil is an important source of N<sub>2</sub>O and CH<sub>4</sub> (Kroon et al., 2010), while ditches plus ditch edges running between dry fields emit CH<sub>4</sub> as well (Peltola et al., 2015). Extending to a larger scale of  $\sim \text{km}^2$ , EC measurements of CH<sub>4</sub> fluxes at 20 m height monitored the emissions from ruminants (Peltola et al., 2015), which were reported to account for the most variabilities of the CH<sub>4</sub> fluxes measured at 6 m, 20 m, and 60 m (Peltola et al., 2015). Isotopic composition measurements reveal that the CH<sub>4</sub> emissions (~ km<sup>2</sup>) are dominated by ruminant emissions with further contributions from the emissions of natural gas and landfills (Röckmann et al., 2016). Large spatial scale (> ha) estimates of N2O emissions in this region are rare and thus far only reported by Hensen et al. (2000) based on morning concentration peaks.

Here, we employed two approaches, the  $^{222}$ Rn tracer method and the vertical gradient method, to independently estimate N<sub>2</sub>O and CH<sub>4</sub> emissions over a one-year the period from 2017 to 2018. The estimated emissions from the two approaches represent different influencing areas, which allows us to assess the influence of the spatial variability on regional estimates. Based on the analysis results, we derived both the annual mean and seasonal variabilities of the surface emissions. Furthermore, we also used the estimates to evaluate the inventories and pinpoint the dominant emissions for different seasons.

#### 2. Materials and methods

#### 2.1. Site characteristics

The Cabauw site with a 213-m meteorological tower (51.971° N,  $4.927^{\circ}$  E, -0.7 m a.s.l.) is located in the western part of the Netherlands. The landscape comprises fields with drainage ditches running between them. These fields are intensively managed grasslands with peat soils, mostly used for dairy farming (Fig. S.1). The major cities in the Netherlands surrounding the site include Utrecht (at a distance of about 20 km), Rotterdam (30 km), The Hague (40 km), and Amsterdam (45 km). Overall,  $\rm N_{2}O$  and  $\rm CH_{4}$  emissions come from mixed agricultural/urban regions.

Soil characteristics are decisive for the  $N_2O$  emission strength, so we briefly describe the surrounding soil. With increasing depth, the soil around the site consists mainly of turf, clay, a mixture of clay and peat, and peat. This soil contains more water in winter and less water in summer. In addition, the soil temperature is lower, about or above  $0\,^{\circ}$ C in winter, and about or above  $20.0\,^{\circ}$ C in summer. Over the 2016-2018 period, the wind mainly came from south to west and the mean wind speeds at  $20\,\text{m}$  and  $200\,\text{m}$  were  $5\,\text{m/s}$ , and  $8\,\text{m/s}$ , respectively; the mean air temperature at the surface was  $11.0\,^{\circ}$ C, with a minimum of  $-10.5\,^{\circ}$ C in winter and a maximum of  $36.0\,^{\circ}$ C in summer; the total rainfall for each year was  $739\,\text{mm}$ ,  $766\,\text{mm}$ , and  $642\,\text{mm}$ , respectively, with the latter value lower than in the other two years due to a drought in the summer of 2018. For more details we refer to (Bosveld et al., 2020; Peltola et al., 2015; Vermeulen et al., 2011).

#### 2.2. Atmospheric measurements

Atmospheric mole fraction measurements of greenhouse gasses and

related tracers have been made at the Cabauw tower ever since 1992. For the period of 2016–2018, a Fourier transform infrared spectroscopy analyzer (Spectronus FTIR) was used to measure the dry air mole factions of CO<sub>2</sub>, CH<sub>4</sub>, CO, and N<sub>2</sub>O at four heights (20 m, 60 m, 120 m, and 200 m). Air was drawn through sampling lines (Synflex 1300) with a flow rate of 10 L min $^{-1}$  using a membrane pump. In addition,  $^{222}\text{Rn}$  concentrations were measured using ANSTO monitors (Zahorowski et al., 2004) at 20 m and 200 m. Hourly vertical concentration profiles of N<sub>2</sub>O, CH<sub>4</sub>, and  $^{222}\text{Rn}$  were used in this study.

#### 2.3. Meteorological observations

The Royal Netherlands Meteorological Institute (KNMI) has been measuring and processing the meteorological data at the Cabauw tower for decades. Three types of datasets are available in the KNMI Data Platform (KDP) (dataplatform.knmi.nl): 'unvalidated', 'validated not gap-filled', and 'validated and gap-filled'. The 'unvalidated' datasets contain the original data obtained from the data logging system; the 'validated not gap-filled' datasets contain the data that have been manually checked and validated, during which some data got rejected based on appropriate constraints: the 'validated and gap-filled' datasets contain the validated data that have been completed by interpolation or modelled values. In this study, we used the 'validated not gap-filled' datasets to determine the fluxes directly from the measurements. The parameters include air temperature, air pressure, sensible heat flux, wind direction, and wind speed. All of these parameters were reported in 10-minute time series. The air temperature and wind direction and speed were all measured at 10 m, 20 m, 40 m, 80 m, 140 m, and 200 m, while the air temperature was also measured at 0.1 m and 2 m. The accuracy of temperature measurements is 0.1 °C. The surface air pressure was reduced to mean sea level and the accuracy is 0.1 hPa. The sensible heat flux was derived from the sonic anemometer/thermometer by means of the EC technique at 3 m, 60 m, 100 m, and 180 m.

#### 2.4. Flux calculation

#### 2.4.1. Vertical gradient method (VGM)

During nighttime, the surface temperature goes down slowly, and a nocturnal boundary layer (NBL) is built up due to temperature inversion. The emitted gasses then become trapped in this boundary layer, causing an increase in the local mole fractions of N2O and CH4. We estimated the average NBL height per night, which was then used to divide the meteorological dataset into two for the flux calculation using the VGM. When the NBL is below 200 m (the highest measurement height level at the Cabauw tower), we used the NBL budget to estimate the surface emissions; when the NBL is above 200 m, we summed the turbulent and storage fluxes to derive the surface emissions. The nighttime was defined considering the time of sunrise and sunset, varying from month to month; in order to choose the period when a stable NBL had developed, the start of nighttime was defined as the time of the sunset plus 1 h, and the end of the nighttime as the time of the sunrise minus 1 h. Here, we selected calm nights when the potential temperature increased with height, and the average NBL height per night was estimated based on the following equation (Arya, 1981),

$$h = 85.1 + 0.089 * \frac{\mathbf{u}_*}{\mathbf{f}} \tag{1}$$

where,  $\mathbf{u}_*$  is the friction velocity measured at surface layer, and f the Coriolis parameter. As shown in the Fig. A.1, the estimated NBL height ranges from tens to hundreds of meters, and is larger in winter months than in summer months.

For the nights with an average NBL height below 200 m, the nocturnal surface flux on a daily scale was calculated using the NBL budget. Assuming advection and turbulence are negligible during calm nights, the fluxes are derived following the equation below (Acevedo et al., 2004; Denmead et al., 1996; Griffis et al., 2013; Herrera et al.,

2021; Mathieu et al., 2005; Pattey et al., 2002; Pattey et al., 2006),

$$F_{\text{surface}} = \int_{0}^{Z_{\text{NBL}}} \frac{1}{V_{\text{m}}} \frac{\partial c}{\partial t} dz = \frac{P}{RT_{\text{air}}} \int_{0}^{Z_{\text{NBL}}} \frac{\partial c}{\partial t} dz$$
 (2)

Where z is the height above soil,  $Z_{NBL}$  is the NBL height,  $V_m$  is the molar volume, t is time, P is atmospheric pressure, R is the ideal gas constant (8.31 J  $K^{-1}$  mol $^{-1}$ ),  $T_{air}$  is air temperature, and  $\frac{\partial c}{\partial t}$  is the change of mole fraction of  $N_2O$  or  $CH_4$  during the night.

We did not apply the NBL budget when the NBL height exceeded our topmost measurement height (200 m) since linearly extrapolating the vertical concentration profiles is prone to underestimation of fluxes. We assumed that there is an "atmospheric box" during calm nights. The surface-atmosphere exchange flux equals the mass trapped within this box (storage flux) and the mass fleeing away from the top of the box (turbulent flux) to the free atmosphere if the advection flux is neglected (Satar et al., 2016; Winderlich et al., 2014). The turbulent flux term closes the budget and makes the height of the integration flexible (within the NBL): in theory, the sum of the storage and turbulent fluxes should be constant with changing integration height (within the NBL). Since we do not have direct eddy flux measurements at the Cabauw tower, the turbulent flux was estimated by the gradient of measured concentration and potential temperature between 200 m and 120 m using the modified Bowen ratio method with sensible heat flux as the tracer (Businger, 1986). As the sensible heat flux used in the turbulent flux calculation was derived at 180 m, the top of the "atmospheric box" was set to 180 m.

The storage flux was determined from the same Eq. (2), except that the upper boundary was set at 180 m. As the concentrations were measured at discrete levels, the vertical profiles of  $N_2O$  and  $CH_4$  mole fractions between consecutive hourly time steps construct trapezoidal areas, and the storage flux can be determined as the sum of those areas (Winderlich et al., 2014). The mole fractions at ground level were linearly extrapolated from those at 20 m and 60 m, and the mole factions at 180 m were linearly interpolated from those at 120 m and 200 m.

The turbulent flux was estimated by the equation below:

$$F_{turbulent} = \frac{H}{C_p M_{Air}} \frac{\Delta c}{\Delta T_{pot}}$$
(3)

where H is the sensible heat flux at 180 m;  $C_p$  the specific heat capacity of air at constant pressure (1.005 J  $g^{-1}$   $K^{-1}$ );  $M_{Air}$  the average molar mass of dry air (28.96 g/mol);  $\Delta T_{pot}$  and  $\Delta c$  are the differences of potential temperature and mole fractions between 120 m and 200 m. The air temperature at 120 m was interpolated linearly from temperature at 140 m and 80 m, based on which the potential temperature at 120 m was derived.

When applying Eq. (3), in some cases, unrealistic turbulent fluxes were generated. Firstly, extremely large and very imprecise numbers are expected if the denominator  $\Delta T_{\text{pot}}$  becomes too small; secondly, the derived fluxes are not valid if the meteorological conditions violate the assumptions for the Bowen ratio similarity method. To filter out such unrealistic outcomes, threshold criteria were established as follows. To solve the problem caused by the denominator  $\Delta T_{pot}$ , the difference between the potential temperatures at two height levels should exceed the instrument precision (Meredith et al., 2014); in this study,  $\Delta T_{pot}$  was set to be larger than 0.2 K. Furthermore, Eq. (3) assumes that the sensible heat flux is evenly distributed along the vertical dimension following Fick's law, so the sensible heat flux has the opposite sign to the difference of potential temperature (Waldo et al., 2019). In addition, despite assuming the turbulence transfers the quantities uniformly, the friction velocity was not included in the criteria to determine if sufficient turbulent conditions exist, because we did not obtained a validated dataset. Several previous studies did not use the friction velocity directly as a criterion either (Denmead et al., 2000; Griffith et al., 2002; Winderlich et al., 2014).

Nighttime observations are suitable for applying the VGM since the

gradient of concentration for the turbulent flux calculation is more reliable during the night than during the day. During daytime, it is very challenging to precisely measure the concentration gradients, because they are often very small within a well-mixed convective boundary layer and may be around or below the instrument precision.

#### 2.4.2. The radon-tracer method (RTM)

The RTM is a well-known technique to derive  $N_2O$  and  $CH_4$  fluxes (Grossi et al., 2018; Van Der Laan et al., 2009) and has been commonly applied to nighttime observations in published studies since daytime observations hardly meet the requirements of the RTM. It is required that  $^{222}$ Rn concentration has a high correlation with the target gas concentration, which happens mostly during night. Assuming that  $^{222}$ Rn and trace gasses share the same diffusivity in the well mixed atmosphere, and that the emission molecules and  $^{222}$ Rn do not instantly engage in a chemical reaction, the fluxes of  $N_2O$  and  $CH_4$  can be derived as follows:

$$F_{N2O~(CH4)} = F_{222Rn} \frac{\Delta N2O~(CH4)}{\Delta_{222Rn}}$$
 (4)

where  $F_{222Rn}$  is the flux of  $^{222}Rn$  and  $\frac{\Delta N20~(CH4)}{\Delta_{222Rn}}$  the slope of the linear regression between the mole fractions of  $N_2O~(CH_4)$  and  $^{222}Rn$  for each night. To keep consistent with the VGM, the same nocturnal window [sunset+1 h, sunrise-1 h] was selected for the calculation per night. The measurement height of the mole fractions used for the RTM was 20 m. To obtain more reliable results, we applied a strict rule that only those events that had an R-squared value larger than 0.7 were selected for flux calculation. After filtering by the R-squared value over the period of 2016-2018, 4 out of 429 events had a negative slope for N2O, and 4 out of 477 events had a negative slope for CH<sub>4</sub>. The negative slope could be caused by either the uptake of N2O and CH4 at the surface, or inflow of air above the planetary boundary layer with a low abundance of <sup>222</sup>Rn. Considering that the major sink of N<sub>2</sub>O and CH<sub>4</sub> is in the atmosphere, and that surface uptake of N2O and CH4 near the Cabauw tower is not very likely, a negative slope was assumed to be caused by diluted  $^{222}\mathrm{Rn}.$ Hence, an assumption of the RTM is that atmospheric transportation of <sup>222</sup>Rn, N<sub>2</sub>O and CH<sub>4</sub> is along the same pathway, and as such cannot produce a negative slope. Therefore, we only selected events with positive slopes. For each night, the minimum number of data points for linear regression was 5.

After <sup>222</sup>Rn is emitted from the soil to the atmosphere, the concentration of <sup>222</sup>Rn will change due to decay and transport of the atmosphere. The time of decay is critical to estimate the correction term (Van Der Laan et al., 2009). While we did not exactly know the transit time of the air mass from the emission point to the Cabauw tower, for a nocturnal window lasting 8–12 h, the change of <sup>222</sup>Rn activity resulting from radioactive decay is only 3–4% (Schmidt et al., 2001). When applying the RTM, (Lopez et al., 2012; Schmidt et al., 2001; Van Der Laan et al., 2009) added the correction factor for the decay, while (Grossi et al., 2018, 2014) did not. Accordingly, we decided to neglect the correction term in determining the fluxes in this study.

The effective  $^{222}$ Rn flux per night in our flux calculations was derived based on the modelled weekly  $^{222}$ Rn flux in Europe with a  $0.5^{\circ} \times 0.5^{\circ}$  grid for the year 2006 (data available at: http://radon.unibas.ch). This gridded European  $^{222}$ Rn flux map was modelled based on an empirical regression between terrestrial gamma-dose rate and  $^{222}$ Rn flux (Szegvary et al., 2009). Its spatial variation is much more significant than temporal variations (Fig. A.2 & Fig. A.3). The  $^{222}$ Rn flux in the Netherlands shows lower values than other countries since the uranium contents of the soils are lower (Table A.1). To eliminate the influence of the heterogeneous distribution of  $^{222}$ Rn fluxes, footprints per night were combined with the  $^{222}$ Rn flux map modelled by Szegvary et al. (2009) to derive the effective  $^{222}$ Rn fluxes per night that was used for the RTM in our study. The yearly average process-based  $^{222}$ Rn flux (Karstens et al., 2015) does not show a significant interannual variability (Fig. A.4),

based on which the  $^{222}$ Rn flux map in 2006 can be used to derive the RTM fluxes during 2017–2018. The effective  $^{222}$ Rn flux per night used for deriving the RTM flux is an average of the  $^{222}$ Rn fluxes of the areas that the wind passed through. Firstly, the transport distance could be roughly estimated based on the mean wind speed per night; this distance was accordingly defined as the radius of a circle with the Cabauw tower as a center. Secondly, the wind direction was evenly divided into four sectors (North indicates  $0^{\circ}$ , and South indicates  $180^{\circ}$ ), and according to the mean wind direction (calculation following circular quantities) per night, we determined the grids that a quarter of the circle would cover. Finally, the mean  $^{222}$ Rn flux of these grids was defined as the effective  $^{222}$ Rn flux per night, which was used in the Eq. (4). The effective daily  $^{222}$ Rn flux did not show a clear seasonal cycle, as shown in Fig. A.5.

#### 2.5. Footprints

The footprint of the VGM fluxes was computed using the flux footprint model developed by Kljun et al. (2015) for turbulent fluxes. When computing this footprint, we should also consider the storage flux, which is not straightforward. In studies about surface-atmosphere exchange, the footprint of the turbulent flux was used to represent the influencing areas of derived surface fluxes (Davis et al., 2003; Desai et al., 2015; Peltola et al., 2015). The difference between the footprints of the storage and turbulent fluxes was therefore ignored.

The footprint of the RTM fluxes can be represented by the concentration footprint at 20 m height considering the theoretical concept of the RTM. It was computed using the atmospheric transport model STILT, implemented at the ICOS Carbon portal (https://www.icos-cp.eu/data-s ervices/tools/stilt-footprint), and aggregated using the interactive Jupyter notebook (https://exploredata.icos-cp.eu/user/username/no tebooks/icos\_jupyter\_notebooks/visualization\_average\_footprints.ip ynb). A 10-day back STILT trajectory Lagrangian transport model with the meteorological conditions represented by hourly operational ECMWF Integrated Forecasting System was used to derive the average footprints with time intervals of 3 h. The STILT footprints can be downloaded from the Carbon Portal (Karstens et al., 2022). They cover 90% of the areas influencing the receptor, i.e. the Cabauw tower. It was not necessary to cover all of the influencing areas since the footprints are too large and sometimes extending to the whole of Europe. In this study, we selected the nocturnal periods from 0:00 to 6:00 o'clock (UTC). We computed aggregated footprints for the full 2017-2018 period, for the grazing months (March-September), and for the non-grazing season months (October-February) to uncover seasonal variations.

#### 2.6. Footprint constrained bottom-up emission inventories

Annual EDGARv6.0 emission grid maps with the spatial resolution of  $0.1^{\circ} \times 0.1^{\circ}$  (Crippa et al., 2020) were used for the comparison with our estimated annual emissions. We calculated the average EDGAR emissions within the influencing area constrained by the VGM flux footprint. The values of gridded EDGARv6.0 emissions vary significantly within the RTM flux footprint; however, this is not the case within the VGM flux footprint (Fig. D.1). Hence, we used two ways to derive average EDGAR emissions: the ordinary arithmetic mean for EDGAR constrained by the VGM flux footprint, and the weighted arithmetic mean for EDGAR constrained by the RTM flux footprint.

From the STILT simulations with the meteorological conditions represented by hourly operational ECMWF Integrated Forecasting System, we obtained the footprints of the RTM fluxes, which provide a quantitative influence of surface emissions at each grid on the enhanced concentration of trace gasses at the receptor, i.e. the Cabauw tower. Based on the footprint, we calculated a weighting factor  $(W_i)$  using the following equation:

$$W_i = \frac{s_i}{\sum_{i}^{n} s_i}$$

where, i indicates each grid of 90% footprints, n the total number of grids of 90% footprints, and  $s_i$  the surface influence of each grid. Hence, the annual EDGARv6.0 emission combined with the 20-m footprints were derived as.

$$\textit{Emission} = \sum_i (emi_iW_i)$$

Where, emi indicates the grid value of the EDGARv6.0 emission map, and i indicates each grid point of the 20-m footprint constrained EDG-ARv6.0 emission map.

Besides the annual mean emissions, monthly EDGARv6.0 grid maps were derived using the high temporal distribution profiles that were disaggregated from yearly regional emissions (Crippa et al., 2020). Combined with the footprints for grazing season months and non-grazing season months, they were also used to determine monthly averaged EDGARv6.0 emissions.

#### 2.7. Uncertainty calculation

The uncertainty of the daily VGM fluxes was determined from the propagation of the measurement errors of each component. The uncertainty of the VGM flux at NBL heights below 200 m,  $U_{below}$ , was determined by the uncertainty in the storage flux,  $U_{stor}$ , while the uncertainty at NBL heights above 200 m,  $U_{above}$ , was calculated as sum in quadrature of the uncertainty of storage fluxes,  $U_{stor}$ , and the uncertainty of turbulent fluxes,  $U_{turbu}$ .

The uncertainties of storage fluxes and turbulent fluxes were calculated as,

$$U_{stor} \; = \; \sqrt{\left(\left(\frac{\varepsilon_P}{P} \; f_{stor}\right)^2 + \left(\frac{\varepsilon_T}{T} \; f_{stor}\right)^2 + \left(\frac{\varepsilon_c}{c} \; f_{stor}\right)^2\right)}$$

and

$$U_{turbu} \; = \; \sqrt{\left(\left(\frac{\mathcal{E}_{H}}{H} \; f_{turbu}\right)^{2} + \left(\frac{\mathcal{E}_{pot}}{pot} \; f_{turbu}\right)^{2} + \left(\frac{\mathcal{E}_{\Delta c}}{\Delta c} \; f_{turbu}\right)^{2}\right)}$$

where,  $\varepsilon_P$ ,  $\varepsilon_T$ ,  $\varepsilon_{pot}$ , and  $\varepsilon_H$  indicate the uncertainty of pressure, temperature, potential temperature, and sensible heat flux, respectively. They were determined as the standard deviation of the hourly dataset averaged from 10-min time series.  $\varepsilon_c$  is the precision of the instrument and is the same for all heights, 0.08 ppb for N<sub>2</sub>O and 0.18 ppb for CH<sub>4</sub>.  $\varepsilon_{\Delta c}$  is the uncertainty of concentration gradients and is calculated as  $\varepsilon_{\Delta c} = \sqrt{\varepsilon_{c_{z1}}^2 + \varepsilon_{c_{z1}}^2}$ . For NBL heights above 200 m, the daily uncertainty of the storage flux and the turbulent flux was firstly derived by summing the hourly uncertainty in quadrature, and then the total daily uncertainty,

 $U_{above}$ , was derived as  $U_{above} = \sqrt{U_{stor}^2 + U_{turbu}^2}$ .

The uncertainty of the daily RTM fluxes was determined by two

components; the uncertainty of  $^{222}$ Rn fluxes,  $\varepsilon$   $_{F_{222Rn}}$ , and the uncertainty of the slope of the linear regression,  $\varepsilon$ <sub>slope</sub>. The uncertainty of the RTM fluxes is derived as,

$$U_{RTM} = \sqrt{\left(\frac{\varepsilon_{F_{222Rn}}}{F_{222Rn}} \ f_{RTM}\right)^2 + \left(\frac{\varepsilon_{slope}}{\mathit{slope}} \ f_{RTM}\right)^2}$$

where  $\varepsilon_{\mathrm{slope}}$  is the standard error of the estimated slope from the linear regression, and  $\varepsilon_{\mathrm{F}_{222\mathrm{Rn}}}$  the standard deviation of the effective  $^{222}\mathrm{Rn}$  fluxes within the footprints per night. Many environmental factors influence the exhalation rate of  $^{222}\mathrm{Rn}$  from soils, such as soil moisture, soil type, and uranium content, leading to variations in the magnitude of the  $^{222}\mathrm{Rn}$  flux. The average modelled  $^{222}\mathrm{Rn}$  fluxes with the standard deviation in the studies for the Netherlands and Europe are shown in Table A.1.

#### 3. Results and discussion

#### 3.1. Vertical profiles

The nocturnal average hourly vertical profiles of  $N_2O$ ,  $CH_4$ , and potential temperature per season for the period of 2017–2018 are shown in Fig. 1. The vertical concentration profiles are presented for heights of 20 m, 60 m, 120 m, and 180 m, based on which the storage flux was estimated. The mole fractions of both  $N_2O$  and  $CH_4$  decrease with altitude in all seasons (except for the  $N_2O$  concentrations at 60 m and 120 m in winter) and the gradients are much smaller in winter than in other seasons, indicating the influence of surface emissions and stratified nocturnal boundary layers.

At 20 m, the concentration increase with time is smallest in winter, as is the potential temperature change. The potential temperature in summer is the highest, followed by that in spring and autumn, with the lowest being in winter. The variance of potential temperature during nocturnal hours is relatively small in winter compared to other seasons. The mole fractions of  $CH_4$  in summer are lowest at 180 m among all seasons because the OH induced atmospheric sink is strongest in summer. The difference between the nocturnal mole fractions of  $N_2O$  and  $CH_4$  between consecutive hours in winter is small, which leads to small storage fluxes.

#### 3.2. Surface fluxes

The fluxes estimated using the VGM and the RTM do not show an interannual variation for either N<sub>2</sub>O or CH<sub>4</sub>, and the RTM flux is more

scattered in winter than in summer (Fig. 2). The mean of the relative total uncertainties of the daily RTM fluxes over the period of 2017–2018 is  $\sim\!44\%$ . The total uncertainty is dominated by the uncertainty of the  $^{222}$ Rn fluxes, and the mean of its relative uncertainties would be  $\sim\!42\%$  when only the uncertainty of the  $^{222}$ Rn fluxes is considered. On the other hand, the uncertainties of daily VGM fluxes are quite variable, with larger values when the NBL is above 200 m than those when the NBL is below 200 m. This is due to the additional term of turbulent fluxes for NBL above 200 m. The relatively large uncertainty of the turbulent fluxes is caused by the uncertainties of the concentration gradient, potential temperature gradient, and sensible heat flux.

In the summer of 2018, the N2O surface fluxes show a few outliers (Fig. 2) because events with abnormally high concentrations occurred on a few nights (Fig. B.1). These could have been caused by the combined effect of heavy precipitation and manure application. At the grassland near the Cabauw tower, the fluxes measured by soil chambers showed spikes during fertilization events in February, May, and September, and the spike fluxes occurred within 2 days after heavy rainfall (Kroon et al., 2008). In another grazing peat grassland, located about 12.5 km northwest of the Cabauw tower, manure and chemical fertilizer were applied from February to October, and the largest 30-min EC flux measured there was around 25 g  $m^{-2}$  yr<sup>-1</sup> (Kroon et al., 2010), which was comparable with the maximum flux estimate of around 30 g  $m^{-2}$  yr<sup>-1</sup> by the RTM. In fact, a number of studies on ecosystem (Liang et al., 2018; Merbold et al., 2014; Mishurov and Kiely, 2010; Phillips et al., 2007) and landscape (Haszpra et al., 2018) scales found that large rainfall/irrigation triggered spike N2O emissions after fertilization. Moreover, it was also found by Liang et al. (2018) that small rain events

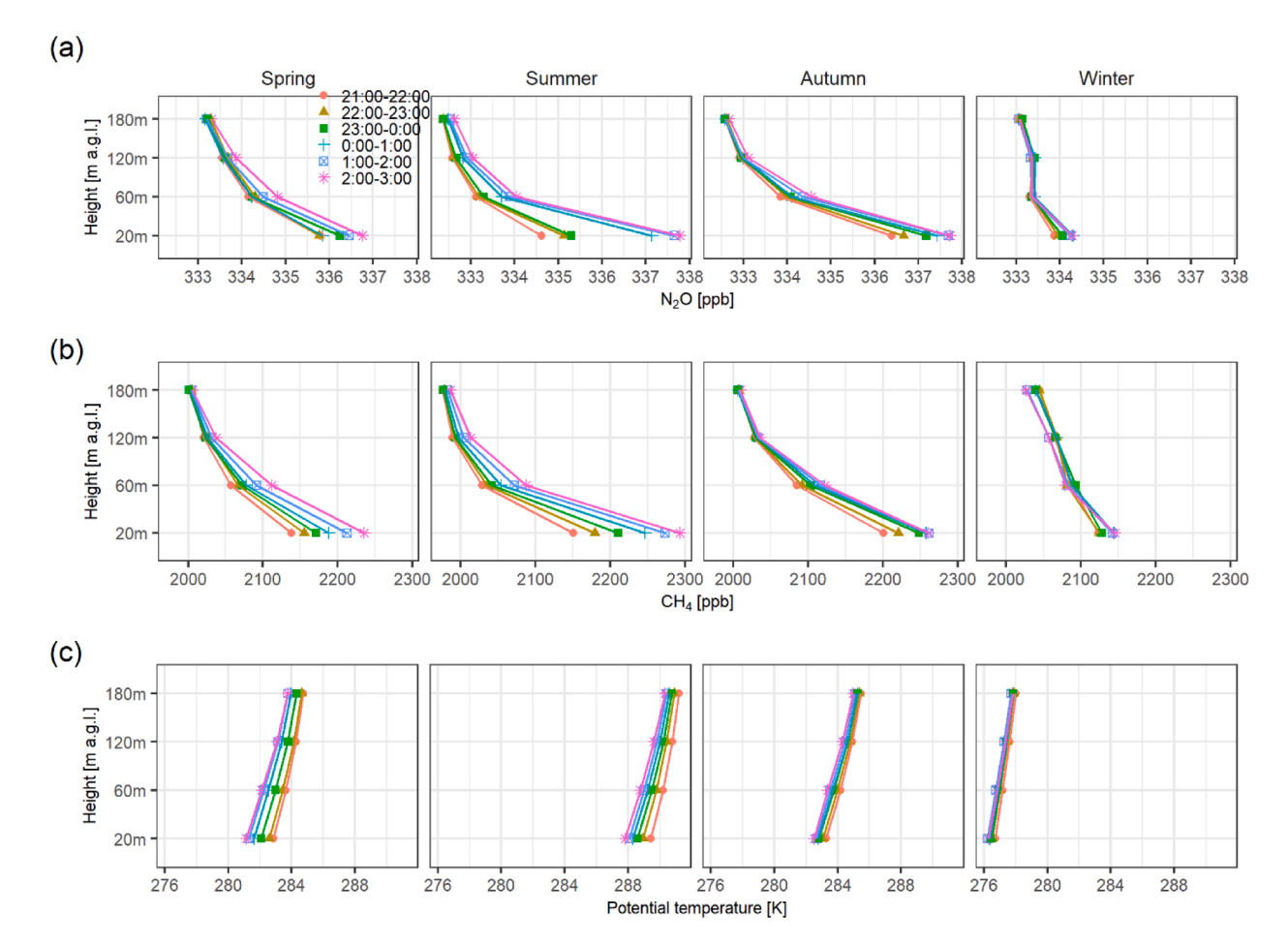
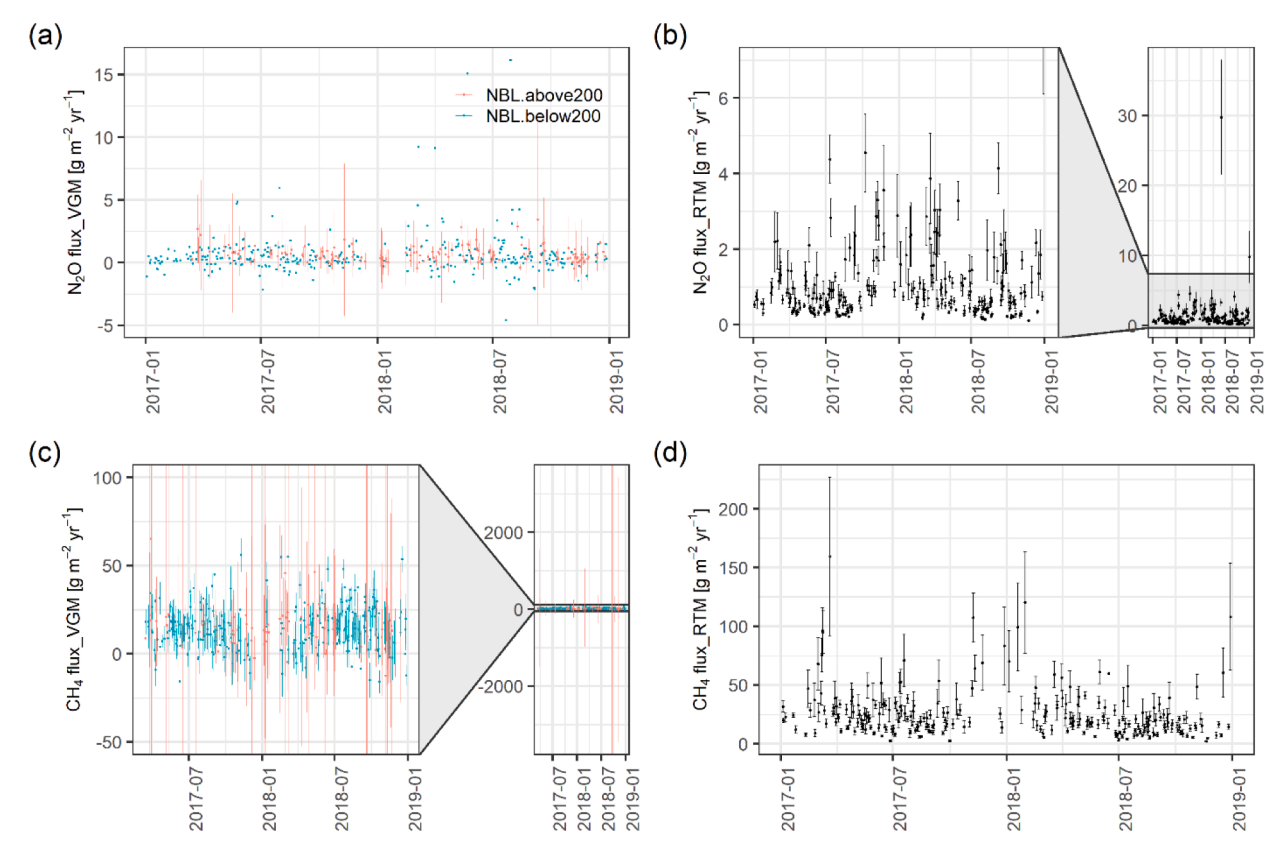


Fig. 1. Average vertical profiles of (a)  $N_2O$  concentration, (b)  $CH_4$  concentration, and (c) potential temperature during 21:00–02:00 UTC for each season during 2017–2018. Different colors indicate different time intervals. Spring indicates March-May, summer indicates June-August, autumn indicates September-November, and winter indicates December-February.



**Fig. 2.** Surface fluxes with uncertainties (error bars) in g  $m^{-2}$  yr<sup>-1</sup> for (a) and (b) N<sub>2</sub>O, and (c) and (d) CH<sub>4</sub> estimated using the VGM (left panel) and RTM (right panel). The colors indicate the VGM fluxes when the NBL height is above (red) and below (blue) 200 m. The RTM fluxes of N<sub>2</sub>O between 0 and ~7 g  $m^{-2}$  yr<sup>-1</sup> and the VGM fluxes of CH<sub>4</sub> between –50 and ~100 g  $m^{-2}$  yr<sup>-1</sup> were zoomed in for clarity.

over a grazing pasture with mixed loam and clay could also trigger  $N_2O$  pulses during a dry summer.

The daily RTM fluxes are lognormally distributed,  $\ln(\text{flux}) \sim N(\mu, \sigma^2)$ , as shown in Fig. B.2. The mode indicated the value occurring most often,  $e^{\mu-\sigma^2}$ , and was selected to obtain the annual RTM flux estimates, as Van Der Laan et al. (2009) did. The number of available nights for the RTM ranges from 3 to 8 for each month in winter, with more available nights in summer (Fig. B.3). The median per month was much lower than the mean in the months with large standard errors, while the median was similar to the mean in the months with small standard errors (Fig. B.3). This is because the mean is sensitive to outliers caused by nearby point sources (Laubach et al., 2015; Van Der Laan et al., 2009).

Table 1 Annual estimates of  $\rm N_2O$  and  $\rm CH_4$  emissions (g  $m^{-2}~\rm yr^{-1})$  using the VGM and the RTM.

| Species | Method | d         | 2017            | 2018                           | Whole<br>period                  |
|---------|--------|-----------|-----------------|--------------------------------|----------------------------------|
| $N_2O$  | VGM    | Mean      | $0.5\pm0.3^{*}$ | $0.7\pm0.4^{\color{red}\star}$ | $\textbf{0.6} \pm \textbf{0.3*}$ |
|         | RTM    | Median    | 0.7 (0.4,       | 0.7 (0.4,                      | 0.7 (0.4,                        |
|         |        |           | 1.1)**          | 1.3)**                         | 1.2)**                           |
|         |        | Lognormal | 0.4 (0.2,       | 0.4 (0.2,                      | 0.4 (0.2,                        |
|         |        | fit       | 2.4)***         | 3.5)***                        | 3.0)***                          |
| $CH_4$  | VGM    | Mean      | 11±5*           | 15±3*                          | 13±4*                            |
|         | RTM    | Median    | 23 (14, 33)**   | 17 (11, 26)**                  | 20 (13, 31)**                    |
|         |        | Lognormal | 14 (7, 71)***   | 11 (5, 60)***                  | 12 (6, 65)***                    |
|         |        | fit       |                 |                                |                                  |

 $<sup>\ ^*</sup>$  The standard deviation indicates the variability of the monthly fluxes within the averaging period;.

The median of the RTM flux is about 75% and 67% higher than the annual estimates obtained from lognormal fits for  $N_2O$  and  $CH_4$  (Table 1).

When comparing the VGM and RTM estimates of annual emissions, we have to consider several factors: 1) the footprint of the RTM fluxes is larger than that of the VGM fluxes; 2) the uncertainty of <sup>222</sup>Rn fluxes causes the uncertainty of the RTM fluxes; 3) the annual VGM estimates are represented by the arithmetic mean, while the annual RTM estimates are represented by the mode of the lognormal fit. The annual mean VGM fluxes are not statistically different from the annual RTM estimates represented by the mode of lognormal fit, and significantly smaller than those represented by the median. Furthermore, differences between the selected datasets used for the two methods may influence the fluxes (Appendix C.1).

#### 3.3. Footprints and flux sources

The footprint difference between VGM and RTM is one of the reasons why the fluxes estimated by the two methods perform differently in the case of our heterogeneous domain. In the 2017–2018 period, footprints were mostly directed towards the west and southwest directions for the VGM and the RTM fluxes. The footprint size of the VGM fluxes is 1–2 orders of magnitude smaller than that of the RTM fluxes (Fig. 3). The 90% footprint maximum of the VGM fluxes is on average 40 km away from the tower, while the 90% footprints of the RTM fluxes extend far beyond the Netherlands.

The 90% footprints of both the VGM and the RTM flux cover agricultural fields and the major cities in the Netherlands (Fig. 3). The main sources of CH<sub>4</sub> are the same for the VGM and the RTM fluxes, including agriculture, landfills, and fossil fuel usage. Agricultural CH<sub>4</sub> emissions come from fertilized soils, manure management, and enteric fermentation (Kroon et al., 2010; Peltola et al., 2015), while urban CH<sub>4</sub> emissions

<sup>\*\*</sup> The range indicates the 25 and 75 percentiles of the fluxes;.

<sup>\*\*\*</sup> The range indicates the 5 and 95 percentiles of the estimated fluxes represented by lognormal fits with 95% confidence interval.

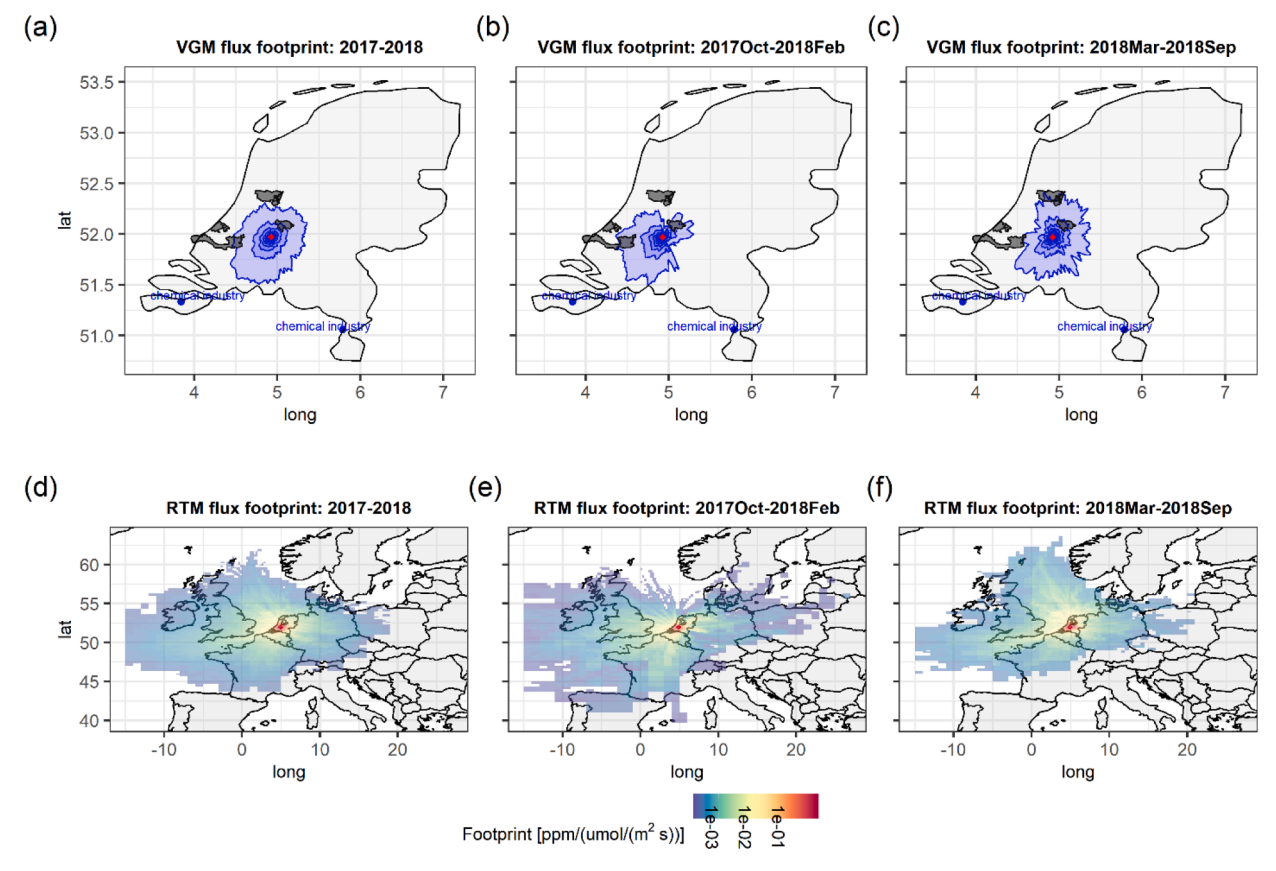


Fig. 3. 90% aggregated footprints during (a) and (d) the whole period 2017–2018, (b) and (e) the non-grazing season months, and (c) and (f) the grazing season months for the fluxes determined using the VGM (top panel) and the RTM (bottom panel). The VGM flux footprint contour lines are presented in the top panel in 10% increments ranging from 10% to 90%, the locations of the Cabauw tower and two chemical industries that emit  $N_2O$  in the plots of VGM flux footprint are presented with red diamond and blue dots, respectively, and the four major cities influencing the VGM flux are shaded with black color. The colorbar in the bottom panel shows the influence of surface emissions on the measured concentrations at the Cabauw tower.

mainly come from landfills and fossil fuel usage.

Different from  $CH_4$ , the main sources of  $N_2O$  are different for the two fluxes. The  $N_2O$  emissions from fertilized soils, manure management, and wastewater treatment are integrated by both the RTM and the VGM fluxes; however, those from chemical industry, located in the furthest south of the Netherlands (Fig. 3), are found within the 90% footprints of the RTM fluxes rather than the VGM fluxes.

#### 3.4. Comparison with fluxes determined on multi-spatial scales

The  $N_2O$  fluxes estimated in this study represent smoothed emissions on a regional scale. The fluxes estimated using the VGM were affected by not only agricultural sources, but also fuel combustion, chemical industry, and waste treatment (Ruyssenaars et al., 2021). The annual fluxes measured by chambers at the Cabauw site were roughly three times our estimated fluxes (Kroon et al., 2008; Velthof et al., 1996), as shown in Fig. 4. This difference is due to the fact that the chambers only measure the highly emitting grazing pastures with peat soils within a few square meters, while our estimates integrate weaker emissions from other sources. In the Netherlands, it was found that peat soils emitted more  $N_2O$  (1.1 – 4.5 times for fertilized grazing pastures) than other types of soils such as clay and sand (Velthof et al., 1996; Velthof and Oenema, 1995). The influencing areas that the estimated fluxes in this study represent cover various soil types; however, the most abundant soils in the Netherlands are sand and clay (Veer, 2006).

Regarding the regional estimates, nighttime  $N_2O$  emissions were estimated from the concentration jump at 200 m from the Cabauw tower, and the average emission of 26 nights during 1995–1996 was 2.3 g  $m^{-2}$  yr<sup>-1</sup> (Hensen et al., 2000). This flux is higher than the fluxes

estimated in this study (Fig. 4), due to the Dutch policy that chemical industry emissions were controlled to decrease since 2006 (van der Maas et al., 2010). For the period from 2017 to 2018, the estimated average annual  $N_2O$  emission from the Dutch inventory is similar to our estimates (Fig. 4). Moreover, the annual  $N_2O$  flux for the Netherlands determined by the RTM in an earlier study by Van Der Laan et al. (2009) was higher than our RTM flux estimate (Fig. 4). We note that the former estimates relate to the period May 2006 to April 2009 when industrial emissions, according to the national emissions inventory estimates (van der Maas et al., 2010), were significantly higher than current levels, due to a decline in 2008.

The emissions of CH<sub>4</sub> show "hotspot" characteristics that are associated with the locations of animals, stored manure, and landfills. EC measurements of the CH<sub>4</sub> flux at 6 m, 20 m, and 60 m at the Cabauw site show that the flux increased with measurement altitude, which was attributed to the fact that high-altitude measurements are dominated by emissions originating from nearby dairy farms while low-altitude measurements represent mainly soil emissions (Peltola et al., 2015). The emissions on hectare scales from fertilized grazing pasture are higher than the VGM fluxes (Kroon et al., 2010). Van Der Laan et al. (2009) determined regional CH4 fluxes directly from atmospheric measurements over the period May 2006 to April 2009, yielding annual estimates that are higher than the VGM fluxes determined in this study (Fig. 4), which is consistent with the decreasing trend from 2006 to 2018 according to the Dutch inventory, although the Dutch inventory estimate based on activity data and emission factors is also higher than the VGM fluxes, as shown in Fig. 4.

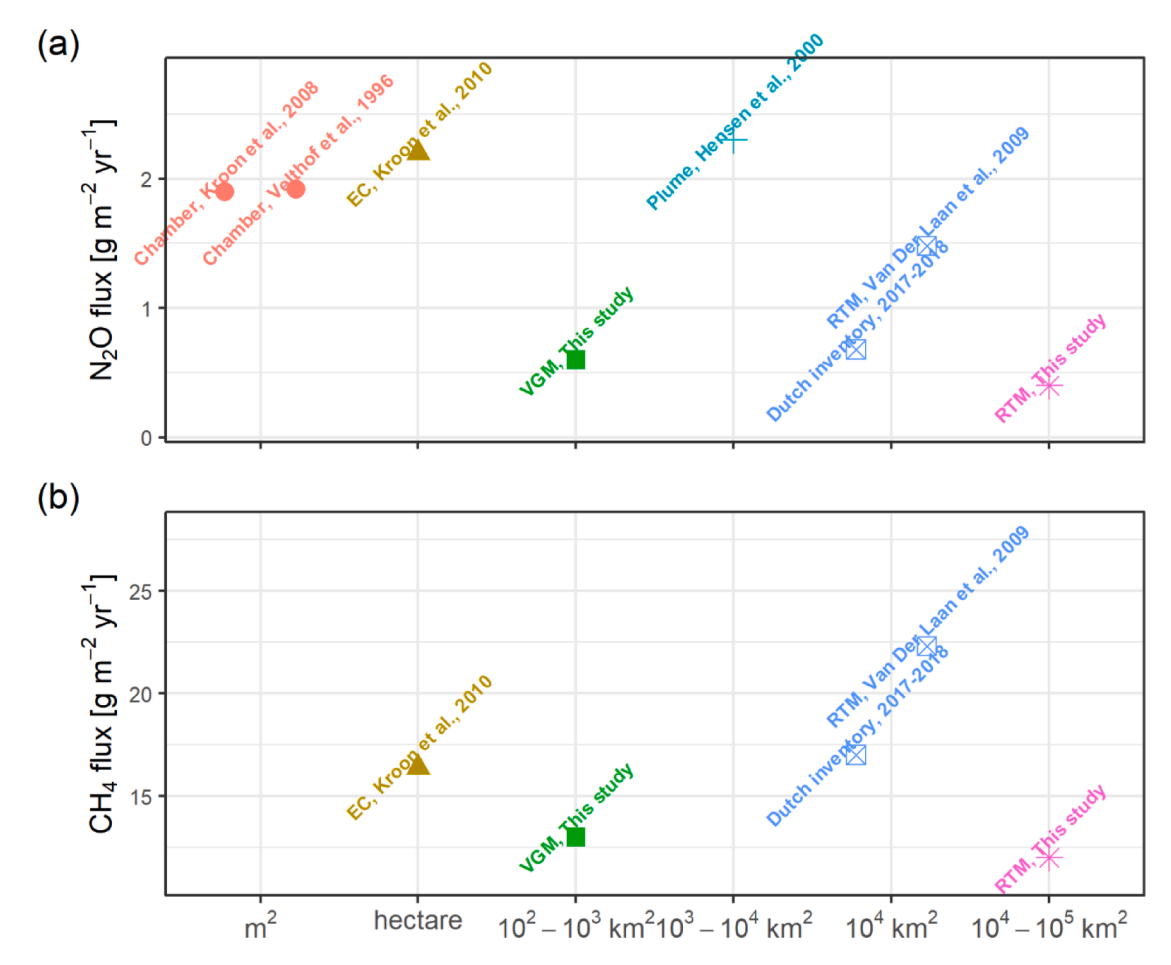


Fig. 4. Annual fluxes of (a)  $N_2O$  and (b)  $CH_4$  reported in this study versus literature values for comparable ecosystems. Different colors highlight different spatial scales.

### 3.5. Comparison of footprint-constrained EDGARv6.0 emissions and estimated fluxes

By checking the exact locations of the chemical plants emitting  $N_2O$  in the Netherlands (Fig. 3), we found that EDGARv6.0 inventory  $N_2O$  emissions from chemical industries are distributed to large areas, which is one of the reasons that EDGAR estimates are higher than the VGM fluxes (Fig. 5a). The 90% footprint of the VGM fluxes does not cover

chemical plants that can emit  $N_2O$ , while the 90% footprint of the RTM fluxes does; consequently, the chemical industries' emissions constrained by the VGM footprint would be much lower than that constrained by the RTM footprint. However, the chemical industries' emissions constrained by the VGM footprint is the largest and higher than that in the RTM footprint-constrained EDGAR emissions (Fig. 5 and Fig. D.2.). Meanwhile, we do not have sufficient proof to determine which other  $N_2O$  sources are also overestimated.

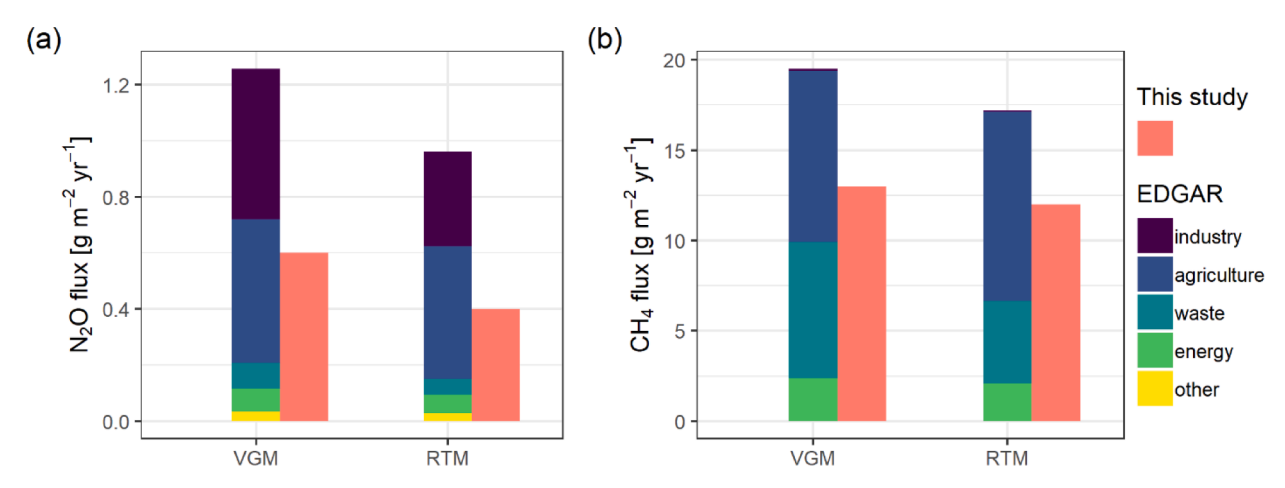


Fig. 5. Comparison of footprint-constrained EDGARv6.0 average emissions and the estimates in our study for (a)  $N_2O$  and (b)  $CH_4$ . The source categories in the EDGARv6.0 inventory are aggregated into five main types according to the Dutch inventory, and the five types include different sources for  $N_2O$  and  $CH_4$ , and in our study domain, the  $CH_4$  emission from the industry category is too small to be shown in the stacked bar.

CH<sub>4</sub> emissions from at least one source sector are over-estimated in EDGARv6.0 inventory compared to our estimated fluxes. The footprintconstrained average EDGARv6.0 emissions are higher than both the VGM and the RTM flux estimates, even knowing that the EDGARv6.0 emission inventories only include anthropogenic emissions and exclude CH<sub>4</sub> emissions from natural sources such as wetlands and inland water systems. The category "agricultural soils" in EDGAR is aggregated into "agriculture" in Fig. 5 and is dominated by rice cultivations for CH<sub>4</sub>. Since there are no rice paddies in the Netherlands, CH<sub>4</sub> emissions from agricultural soils in EDGAR are therefore almost zero (Fig. D.3). However, fertilized peat soils (Kroon et al., 2010) and drainage ditches (Schrier-Uijl et al., 2010) in similar ecosystems to ours have been reported to emit CH<sub>4</sub>, which are not included in EDGARv6.0 inventory, but they are in our estimated fluxes. It has to be noticed that the EDGAR inventory of N2O and CH4 is very uncertain for some sectors due to inaccurate and/or missing information of activity data statistics. The emissions of N2O and CH4 from agriculture and waste are the most uncertain; the relative uncertainty is in the range of 35% - 134% for CH<sub>4</sub>, and 10% – 400% for N<sub>2</sub>O (Solazzo et al., 2021).

#### 3.6. Seasonal variations

We present seasonal variations of the  $N_2O$  and  $CH_4$  fluxes based on only our VGM estimates. The RTM estimates were not considered due to a lack of statistics. The available nights for the RTM in winter months are limited, which may lead to potentially biased monthly mean fluxes.

#### 3.6.1. N<sub>2</sub>O

The estimated monthly  $N_2O$  surface fluxes vary between 0.2 and 1.1 g  $m^{-2}$  yr $^{-1}$  (Fig. 6). The average surface flux of 0.7 g  $m^{-2}$  yr $^{-1}$  for grazing months (March – September) is higher than that of 0.4 g  $m^{-2}$  yr $^{-1}$  for non-grazing months (October – February). However, the average footprint-constrained EDGARv6.0 emission estimates of  $N_2O$  do not show a seasonal variation. Tower measurements of  $N_2O$  fluxes focusing on mixed agricultural urban regions are limited and reported consistent seasonal variations with ours (Griffis et al., 2013; Haszpra et al., 2018). Long-term tower measurements over urban areas are even more scarce; as far as we are aware, only Järvi et al. (2014) reported urban EC fluxes, for the city of Helsinki over the months of June to November, and did not find any seasonal variation.

#### 3.6.2. CH₄

The monthly CH<sub>4</sub> surface fluxes estimated by the VGM show a smaller seasonal variation than N<sub>2</sub>O, varying from 9 to 18 g  $m^{-2}$  yr<sup>-1</sup> (Fig. 6). The average surface flux for grazing months (15 g  $m^{-2}$  yr<sup>-1</sup>) is higher than that for non-grazing months (10 g  $m^{-2}$  yr<sup>-1</sup>). The average

footprint-constrained EDGARv6.0 emissions, on the other hand, do not show a seasonal variation. The estimated  $\mathrm{CH_4}$  fluxes using the VGM in this study represent an area of roughly  $\sim \! 10^2 \ \mathrm{km^2}$  and integrate the emissions mainly from ruminants, peat soils, waste management, and energy usage. Long-term tall tower measurements of  $\mathrm{CH_4}$  fluxes commonly focused on forests and wetlands, which are not comparable to the VGM fluxes measured in our case. The emissions from urban regions have been reported to show seasonal variations opposite to ours (i.e., higher in winter than in summer), which was attributed to the fossil fuel combustion (Helfter et al., 2016; Huang et al., 2019). The emissions from similar agricultural ecosystems show a seasonal variation consistent with ours, but were measured on  $\sim \! m^2$  and hectare scales (Kroon et al., 2010; Mathot et al., 2012).

#### 3.7. Environmental drivers of the regional fluxes of N2O and CH4

We investigated the correlation between several environmental factors and the estimated fluxes. The surface air temperature was found to be positively correlated with the VGM fluxes for CH $_4$  but not for N $_2$ O (Fig. 7). The air temperature was also reported to drive the monthly regional fluxes of N $_2$ O (Griffis et al., 2017) and CH $_4$  (Desai et al., 2015; Helfter et al., 2016). Although the coupling of soil temperature and soil moisture influences the soil emissions of N $_2$ O and CH $_4$ , in our study, the regional fluxes estimated by the VGM were not controlled by either since the VGM fluxes integrate multiple source emissions, not only the soil emissions. In addition, soil water content was also found to be significantly correlated with the RTM fluxes. Soil moisture was reported to predominantly influence the seasonal variations of  $^{222}$ Rn exhalation (Schwingshackl, 2013; Karstens et al., 2015), and the RTM was established on the high correlation of target species and  $^{222}$ Rn, so the fluxes estimated by the RTM are inherently influenced by soil water content.

#### 4. Discussion

#### 4.1. Dominant sources of seasonal variations

The seasonal variations of the VGM fluxes are determined by both the relative contribution and the seasonal amplitude of each emission source. Due to the limitation of the methodology, we are not able to perform a source attribution. However, based on the calculated footprints, we can analyze the source types that contribute to the derived fluxes. In the following subsections, we discuss the seasonal variation of multiple source emissions and analyze the dominant sources that lead to the seasonal variation of the VGM fluxes for  $N_2O$  and  $CH_4$ .

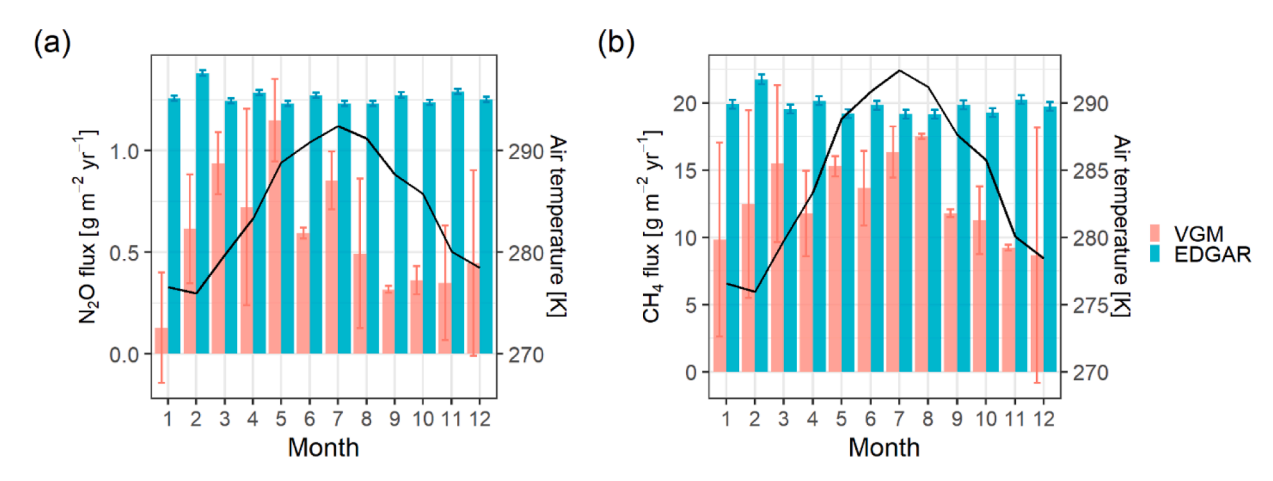


Fig. 6. Aggregated monthly fluxes estimated by the VGM (red) and aggregated monthly EDGARv6.0 emissions constrained by the flux footprint (blue) during the period of 2017–2018 for (a)  $N_2O$  and (b)  $CH_4$ .

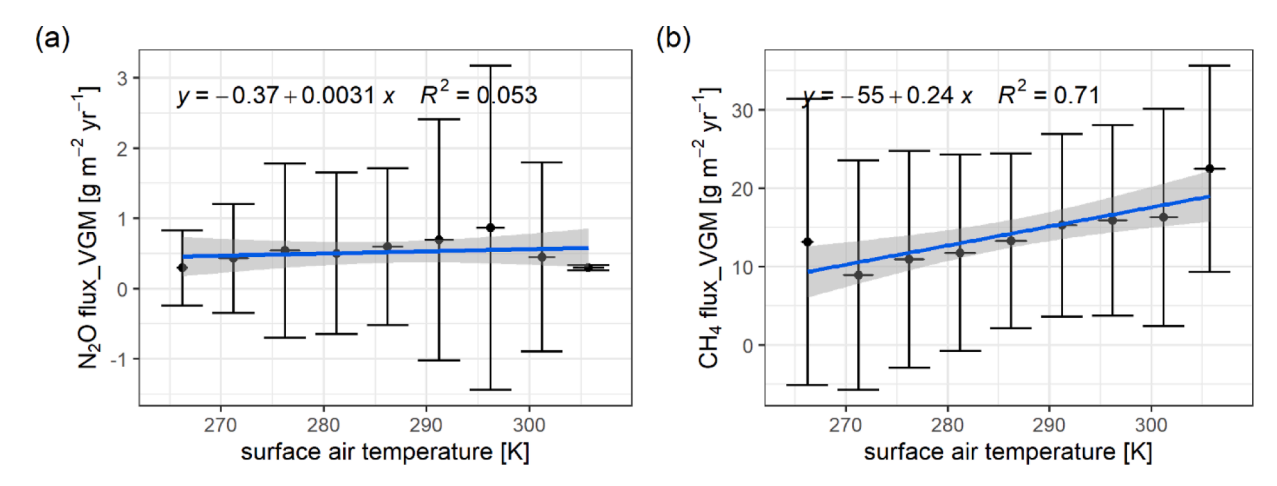


Fig. 7. The fluxes of (a) N<sub>2</sub>O and (b) CH<sub>4</sub> obtained from VGM as a function of surface air temperature from 2017 to 2018. The surface air temperature is averaged per 5 Kelvin. Blue lines and equations represent linear regressions.

#### 4.1.1. N<sub>2</sub>O

The seasonal variation of the VGM N2O fluxes is most likely dominated by agricultural emissions that come from peat soils and manure management. The footprints of the VGM fluxes cover both agricultural and urban emissions. A seasonal variation (i.e., higher fluxes in grazing months than in non-grazing months) of agricultural N2O emissions from similar grazing grasslands has been widely reported on smaller spatial scales.  $N_2O$  fluxes measured on a scale of  $\sim m^2$  were reported to show a larger seasonal variation than that of our VGM estimates, from 0.7 to 4.2 g  $m^{-2}$  yr<sup>-1</sup> (Velthof et al., 1996); spike N<sub>2</sub>O fluxes on a hectare scale were found from February to October when several fertilization and harvest events occurred (Kroon et al., 2010). Furthermore, N2O emissions from a commercial dairy farm were also found to be high in warm seasons and low in cold seasons (Leytem et al., 2011). The urban emissions integrated by the VGM fluxes mainly come from wastewater treatment. A wastewater treatment plant located near the city of Rotterdam (within the 90% footprint) emitted N2O with a seasonal variation that is consistent with ours, and an amplitude of less than 0.1 g  $m^{-2}$ yr<sup>-1</sup> (Daelman et al., 2015), which is much smaller than that of agricultural emissions. The influence of the wastewater treatment emissions on the VGM fluxes should be smaller than that of agricultural emissions due to larger distances from the Cabauw tower. Taken together, the seasonal variation of wastewater treatment emissions is not likely to dominate the VGM flux's seasonal variations.

#### 4.1.2. CH<sub>4</sub>

The observed seasonal variation of CH<sub>4</sub> emissions, with high values during grazing months (Fig. 6), reflects seasonal agricultural activities. The agricultural sources in our study domain include peat soils, manure management, and enteric fermentation. The emissions from intensively managed grasslands have been reported to show a seasonal variation that is consistent with our observations (Kroon et al., 2010; Schrier-Uijl et al., 2010). Manure management could emit more CH<sub>4</sub> in grazing months when the temperature is higher than in non-grazing months (Husted, 1994; Mathot et al., 2012). The seasonal variation of enteric emissions is influenced by multiple factors including breeding status, feed quality, and management regimes (Lassey, 2007); even opposite seasonal variations have been reported for different conditions (Ulvatt et al., 2002). Enteric emissions are strongly related to the number of animals (Dumortier et al., 2017) and decrease with concentrate share in their diet (Mathot et al., 2012). The number of livestock in the Netherlands decreased by 2% and 5% from April to December for 2017 and 2018, respectively (data source: https://opendata.cbs.nl/#/CBS/en /dataset/80274eng/table?searchKeywords=cow), and a change of the concentrate in the diet of cattle in the Netherlands was not found. Taken together, only a small seasonal variation of regional CH<sub>4</sub> emission from

enteric fermentation is expected, if at all. Furthermore, based on the footprint, the VGM fluxes integrated the urban emissions that have two major sources, landfills and fossil fuel use. These two sources are reported to have the opposite seasonal variation to what we observe (Börjesson and Svensson, 1997; Chanton and Liptay, 2000; Hensen and Scharff, 2001; Huang et al., 2019). Therefore, any potential contribution of the two sources to the observed seasonal variation is not significant compared to that of the agricultural source.

#### 4.2. Diurnal cycle of regional fluxes

Regional fluxes of  $N_2O$  and  $CH_4$  do not necessarily show a diurnal cycle because they integrate multiple source emissions that may have opposite diurnal cycles. As mentioned above, the RTM fluxes of both  $N_2O$  and  $CH_4$  were logically found to be correlated with soil water content. The change of soil water content can be used to infer the diurnal cycle of the RTM fluxes. However, the diurnal cycle of soil water content is not observed as shown in Fig. A.6, and it reflects that the diurnal cycle of the RTM fluxes would not be observed either.

To infer the diurnal cycle of estimated VGM CH<sub>4</sub> fluxes, we analyzed the diurnal cycle of surface air temperature. As shown in Fig. A.6, the difference between daytime and nighttime temperatures ranges from 2.5 °C to 8 °C for the whole year. Based on the linear regression equation in Fig. 7, the daytime CH<sub>4</sub> fluxes would be around 1–2 g  $m^{-2}$  yr<sup>-1</sup> larger than the nighttime fluxes. Therefore, the calculated daily average would be underestimated by 0.5–1 g  $m^{-2}$  yr<sup>-1</sup>, or by about 3–7% of the annual mean fluxes.

Surface air temperature was not found to control the VGM  $N_2O$  fluxes. The diurnal cycle of them also depends on both the strength of the diurnal cycle of each source emission and its proportion in the total emissions. The emissions of  $N_2O$  from agricultural soils are spatially variable and region-specific. Wu et al. (2021) reviewed the literature and found that among the studies over grassland soils (which is a similar soil type as our site), around 82% reported daytime peaking of  $N_2O$ , versus 7% nighttime peaking. However, a diurnal cycle was not found over a grazing grassland that has similar climate and managements to ours (Kroon et al., 2010). The diurnal cycle of  $N_2O$  emissions from manure management (i.e., composting) was reported to be unclear (Leytem et al., 2011). The  $N_2O$  emissions from wastewater treatment plant peak around midnight (Daelman et al., 2015), opposite from the diurnal cycle of soil chamber measurements.

#### 4.3. Towards mitigation of agricultural emissions of N2O and CH4

The  $N_2O$  and  $CH_4$  estimates in our study come from various sources, among which agricultural emissions are influenced by environmental

factors, such as air temperature, soil temperature/moisture, precipitation, and soil micro-organisms. For  $CH_4$ , the agricultural source that is most sensitive to environmental factors is stored manure; for  $N_2O$ , it is manure that is stored outside/in a tank and applied in the fields (the latter generating much more  $N_2O$  than the former). To reduce the combined greenhouse gas (GHG) effect of the emissions of  $N_2O$  and  $CH_4$ , the timing with which manure is stored or applied to the fields is important, possibly in a region-specific fashion.

Previous studies on plot/field scales reported that stored fresh manure generates less CH4 and N2O in grazing seasons than in nongrazing seasons. In our study area, the VGM fluxes of CH4 have a strong positive correlation with surface air temperature, but this is not the case with the N2O fluxes (Fig. 7). This indicates that, even on regional scales, the CH<sub>4</sub> emissions from stored manure increase with air temperature. Considering the single factor of air temperature only, manure should be stored in cold seasons to mitigate the combined GHG effect of N2O and CH4. Furthermore, precipitation can trigger very high N<sub>2</sub>O emissions after manure is applied to the fields (Haszpra et al., 2018; Liang et al., 2018; Merbold et al., 2014; Mishurov and Kiely, 2010; Phillips et al., 2007); as a result, manure should not be applied to fields in rainy seasons. However, the ideal environmental conditions for reducing the combined GHG effect of N<sub>2</sub>O and CH<sub>4</sub> will likely depend on the actual climate of different regions, as well as other region-specific features; for example, during warm season months in the Netherlands, many animals are grazing outside, freely spreading manure. Hence, to identify the good timing to apply manure to fields artificially, the seasonal variations of agricultural emissions of N2O and CH4 should be studied, and the mitigation measures may well be a trade-off between the mitigation of N<sub>2</sub>O and CH<sub>4</sub> emissions.

#### Conclusions

This study presents the magnitude and seasonal variations of emission estimates of  $N_2O$  and  $CH_4$  over a mixed agriculture-urban area. The surface fluxes were determined from atmospheric measurements at the Cabauw tall tower using two independent approaches and compared with the EDGARv6.0 emission inventory.

We found that the annual RTM estimates represented by the mode of lognormal fit for N<sub>2</sub>O and CH<sub>4</sub> are 0.4 g  $m^{-2}$  yr $^{-1}$  and 12 g  $m^{-2}$  yr $^{-1}$ , and the VGM estimates are 0.6  $\pm$  0.3 g  $m^{-2}$  yr $^{-1}$  and 13  $\pm$  4 g  $m^{-2}$  yr $^{-1}$ , respectively. The estimates are smaller than the average Dutch inventory estimate of 0.7 g m<sup>-2</sup> yr<sup>-1</sup> for N<sub>2</sub>O and 17 g  $m^{-2}$  yr<sup>-1</sup> for CH<sub>4</sub> during 2017-2018. Furthermore, the average EDGARv6.0 emissions constrained by the VGM and the RTM footprints are 1.3 g  $m^{-2}$  yr<sup>-1</sup> and  $0.9 \text{ g } m^{-2} \text{ yr}^{-1} \text{ for N}_2\text{O}, \text{ and 21 g } m^{-2} \text{ yr}^{-1} \text{ and 18 g } m^{-2} \text{ yr}^{-1} \text{ for CH}_4.$ Compared to our estimated fluxes, EDGARv6.0 N2O and CH4 emissions are both overestimated; for N2O, it is mainly caused by an overestimation of the chemical industry's emission. In contrast to EDGARv6.0's nearly constant monthly emissions throughout the year, the emissions estimated by the VGM show monthly variations, ranging from 0.2 to 1.1 g  $m^{-2}$  yr<sup>-1</sup> for N<sub>2</sub>O and from 9 to 18 g  $m^{-2}$  yr<sup>-1</sup> for CH<sub>4</sub>. Seasonal variations are observed for both N2O and CH4, with relatively high values, 0.7 and 15 g m<sup>-2</sup> yr<sup>-1</sup>, during grazing months (March to September) and relatively low values, 0.4 and 10 g m<sup>-2</sup> yr<sup>-1</sup>, during nongrazing months (October to February), which is most likely caused by agricultural emissions. This study demonstrates that nighttime vertical concentration profile measurements at a tall tower can be used to constrain both the mean emissions of N2O and CH4 and the temporal variations of their emissions on a regional scale. To mitigate the combined agricultural emissions of N2O and CH4, it would be helpful to investigate further the seasonal variations with environmental factors to determine the good timing for applying manure to the fields.

#### **Declaration of Competing Interest**

The authors declare that they have no known competing financial

interests or personal relationships that could have appeared to influence the work reported in this paper

#### Data availability

Data will be made available on request.

#### Acknowledgments

This work was supported by the National Key Research and Development Program of China under grant 2022YFE0209100, and has been accomplished by using data generated in the Ruisdael Observatory, a scientific infrastructure co-financed by the Dutch Research Council (NWO, grant number 184.034.015). The authors would like to thank Ute Karstens and Ida Storm for providing the footprints, and Natascha Kljun for making the Flux Footprint Prediction code available. Furthermore, Xin Tong is grateful to the funding from China Scholarship Council (CSC) and from the University of Groningen.

#### Supplementary materials

Supplementary material associated with this article can be found, in the online version, at doi:10.1016/j.agrformet.2023.109433.

#### References

- Acevedo, O.C., Moraes, O.L., Da Silva, R., Fitzjarrald, D.R., Sakai, R.K., Staebler, R.M., Czikowsky, M.J., 2004. Inferring nocturnal surface fluxes from vertical profiles of scalars in an Amazon pasture. Glob. Chang. Biol 10 (5), 886–894.
- Alvarez, R.A., Zavala-Araiza, D., Lyon, D.R., Allen, D.T., Barkley, Z.R., Brandt, A.R., Davis, K.J., Herndon, S.C., Jacob, D.J., Karion, A., Kort, E.A., Lamb, B.K., Lauvaux, T., Maasakkers, J.D., Marchese, A.J., Omara, M., Pacala, S.W., Peischl, J., Robinson, A.L., Shepson, P.B., Sweeney, C., Townsend-Small, A., Wofsy, S.C., Hamburg, S.P., 2018. Assessment of methane emissions from the U.S. oil and gas supply chain. Science 361 (6398), 186–188.
- Arya, S.P.S., 1981. Parameterizing the height of the stable atmospheric boundary layer. J. Appl. Meteorol. Climatol. 20 (10), 1192–1202.
- Börjesson, G., Svensson, B.H., 1997. Seasonal and diurnal methane emissions from a landfill and their regulation by methane oxidation. Waste Manag. Res. 15 (1), 33–54.
- Bosveld, F.C., Baas, P., Beljaars, A.C.M., Holtslag, A.A.M., de Arellano, J.V.G., van de Wiel, B.J.H., 2020. Fifty years of atmospheric boundary-layer research at Cabauw serving weather, air quality and climate. Boundary-Layer Meteorol 177 (2), 583–612.
- Businger, J.A., 1986. Evaluation of the accuracy with which dry deposition can be measured with current micrometeorological techniques. J. Clim. Appl. Meteorol. 25 (8), 1100–1124.
- Chanton, J., Liptay, K., 2000. Seasonal variation in methane oxidation in a landfill cover soil as determined by an in situ stable isotope technique. Glob. Biogeochem. Cycles. 14 (1), 51–60.
- Crippa, M., Solazzo, E., Huang, G., Guizzardi, D., Koffi, E., Muntean, M., Schieberle, C., Friedrich, R., Janssens-Maenhout, G., 2020. High resolution temporal profiles in the emissions database for global atmospheric research. Sci. Data 7 (1), 1–17.
- Daelman, M.R.J., van Voorthuizen, E.M., van Dongen, U.G.J.M., Volcke, E.I.P., van Loosdrecht, M.C.M., 2015. Seasonal and diurnal variability of N<sub>2</sub>O emissions from a full-scale municipal wastewater treatment plant. Sci. Total Environ. 536, 1–11.
- Davis, K.J., Bakwin, P.S., Yi, C., Berger, B.W., Zhao, C., Teclaw, R.M., Isebrands, J.G., 2003. The annual cycles of CO<sub>2</sub> and H<sub>2</sub>O exchange over a northern mixed forest as observed from a very tall tower. Glob. Chang. Biol. 9, 1278–1293.
- Denmead, O.T., Leuning, R., Jamie, I., Griffith, D.W.T., 2000. Nitrous oxide emissions from grazed pastures: measurements at different scales. Chemosph. - Glob. Chang. Sci. 2 (3–4), 301–312.
- Denmead, O.T., Raupach, M.R., Dunin, F.X., Cleugh, H.A., Leuning, R., 1996. Boundary layer budgets for regional estimates of scalar fluxes. Glob Chang Biol 2 (3), 255–264.
- Desai, A.R., Xu, K., Tian, H., Weishampel, P., Thom, J., Baumann, D., Andrews, A.E., Cook, B.D., King, J.Y., Kolka, R., 2015. Landscape-level terrestrial methane flux observed from a very tall tower. Agric. For. Meteorol. 201, 61–75.
- Dumortier, P., Aubinet, M., Beckers, Y., Chopin, H., Debacq, A., Gourlez de la Motte, L., Jérôme, E., Wilmus, F., Heinesch, B., 2017. Methane balance of an intensively grazed pasture and estimation of the enteric methane emissions from cattle. Agric. For. Meteorol. 232, 527–535.
- Eckl, M., Roiger, A., Kostinek, J., Fiehn, A., Huntrieser, H., Knote, C., Barkley, Z.R., Ogle, S.M., Baier, B.c., Sweeney, C., Davis, K.J., 2021. Quantifying nitrous oxide emissions in the US Midwest: a top-down study using high resolution airborne in-situ observations. Geophys. Res. Lett. 48 (5).
- Fu, C., Lee, X., Griffis, T.J., Dlugokencky, E.J., Andrews, A.E., 2017. Investigation of the  $N_2O$  emission strength in the U. S. Corn Belt. Atmos. Res. 194, 66–77.

- Ganesan, A.L., Manning, A.J., Grant, A., Young, D., Oram, D.E., Sturges, W.T., Moncrieff, J.B., O'Doherty, S., 2015. Quantifying methane and nitrous oxide emissions from the UK and Ireland using a national-scale monitoring network. Atmos. Chem. Phys. 15, 6393–6406.
- Griffis, T.J., Chen, Z., Baker, J.M., Wood, J.D., Millet, D.B., Lee, X., Venterea, R.T., Turner, P.A., 2017. Nitrous oxide emissions are enhanced in a warmer and wetter world. Proc. Natl. Acad. Sci. 114, 12081–12085.
- Griffis, T.J., Lee, X., Baker, J.M., Russelle, M.P., Zhang, X., Venterea, R., Millet, D.B., 2013. Reconciling the differences between top-down and bottom-up estimates of nitrous oxide emissions for the U.S. Corn Belt. Glob. Biogeochem. Cycles 27 (3), 746–754.
- Griffith, D.W.T., Leuning, R., Denmead, O.T., Jamie, I.M., 2002. Air-land exchanges of CO<sub>2</sub>, CH<sub>4</sub> and N<sub>2</sub>O measured by FTIR spectrometry and micrometeorological techniques. Atmos. Environ. 36 (11), 1833–1842.
- Grossi, C., Voge, F.R., Morgui, J.A., Curcoll, R., Águeda, A., Batet, O., Nofuentes, M., Occhipinti, P., Vargas, A., Rodó, X., 2014. First estimation of CH<sub>4</sub> fluxes using the<sup>222</sup>Rn tracer method over the central Iberian peninsula. WIT Trans. Ecol. Environ. 183, 233–245.
- Grossi, C., Vogel, F.R., Curcoll, R., Àgueda, A., Vargas, A., Rodó, X., Morguí, J.-A., 2018. Study of the daily and seasonal atmospheric  $CH_4$  mixing ratio variability in a rural Spanish region using  $^{222}$ Rn tracer. Atmos. Chem. Phys. 18 (8), 5847–5860.
- Haszpra, L., Hidy, D., Taligás, T., Barcza, Z., 2018. First results of tall tower based nitrous oxide flux monitoring over an agricultural region in Central Europe. Atmos. Environ. 176, 240–251.
- Helfter, C., Tremper, A.H., Halios, C.H., Kotthaus, S., Bjorkegren, A., Grimmond, C.S.B., Barlow, J.F., Nemitz, E., 2016. Spatial and temporal variability of urban fluxes of methane, carbon monoxide and carbon dioxide above London, UK. Atmos. Chem. Phys. 16. 10543–10557.
- Hensen, A., Scharff, H., 2001. Methane emission estimates from landfills obtained with dynamic plume measurements. Water, Air Soil Pollut. Focus 1 (5), 455–464.
- Hensen, A., Villar, A.D., Vermeulen, A.T., 2000. Emission estimates based on ambient N<sub>2</sub>O concentrations measured at a 200m high tower in the Netherlands 1995–1997. Non-CO<sub>2</sub> greenhouse gases: scientific understanding. Control and Implementation 153–158.
- Herrera, S.A., Diskin, G.S., Harward, C., Sachse, G., De Wekker, S.F., Yang, M., Choi, Y., Wisthaler, A., Mallia, D.V., Pusede, S.E., 2021. Wintertime nitrous oxide emissions in the San Joaquin valley of California estimated from aircraft observations. Environ. Sci. Technol. 55 (8), 4462–4473.
- Huang, J., Golombeck, A., Prinn, R., Weiss, R., Fraser, P., Simmonds, P., Dlugokencky, E. J., Hall, B., Elkins, J., Steele, P., Langenfelds, R., Krummel, P., Dutton, G., Porter, L., 2008. Estimation of regional emissions of nitrous oxide from 1997 to 2005 using multinetwork measurements, a chemical transport model, and an inverse method. J. Geophys. Res. Atmos. 113. 1–19.
- Huang, Y., Kort, E.A., Gourdji, S., Karion, A., Mueller, K., Ware, J., 2019. Seasonally resolved excess urban methane emissions from the Baltimore/Washington, DC metropolitan region. Environ. Sci. Technol. 53 (19), 11285–11293.
- Husted, S., 1994. Seasonal variation in methane emission from stored slurry and solid manures. J. Environ. Qual. 23 (3), 585–592.
- Järvi, L., Nordbo, A., Rannik, Ü., Haapanala, S., Mammarella, I., Pihlatie, M., Vesala, T., Riikonen, A., 2014. Urban nitrous-oxide fluxes measured using the eddy-covariance technique in Helsinki, Finland. Boreal Environ. Res. 19, 108–121.
- Jeong, S., Zhao, C., Andrews, A.E., Dlugokencky, E.J., Sweeney, C., Bianco, L., Wilczak, J.M., Fischer, M.L., 2012. Seasonal variations in N<sub>2</sub>O emissions from central California. Geophys. Res. Lett. (16), 39.
- Karion, A., Sweeney, C., Kort, E.A., Shepson, P.B., Brewer, A., Cambaliza, M., Conley, S. A., Davis, K., Deng, A., Hardesty, M., Herndon, S.C., Lauvaux, T., Lavoie, T., Lyon, D., Newberger, T., Pétron, G., Rella, C., Smith, M., Wolter, S., Yacovitch, T.I., Tans, P., 2015. Aircraft-based estimate of total methane emissions from the Barnett shale region. Environ. Sci. Technol. 49 (13), 8124–8131.
- Karstens, U., Schwingshackl, C., Schmithüsen, D., Levin, I., 2015. A process-based 222 radon flux map for Europe and its comparison to long-term observations. Atmos. Chem. Phys. 15 (22), 12845–12865.
- Kirschke, S., Bousquet, P., Ciais, P., Saunois, M., Canadell, J.G., Dlugokencky, E.J., Bergamaschi, P., Bergmann, D., Blake, D.R., Bruhwiler, L., Cameron-Smith, P., Castaldi, S., Chevallier, F., Feng, L., Fraser, A., Heimann, M., Hodson, E.L., Houweling, S., Josse, B., Fraser, P.J., Krummel, P.B., Lamarque, J.-F., Langenfelds, R. L., Le Quéré, C., Naik, V., O'Doherty, S., Palmer, P.I., Pison, I., Plummer, D., Poulter, B., Prinn, R.G., Rigby, M., Ringeval, B., Santini, M., Schmidt, M., Shindell, D. T., Simpson, I.J., Spahni, R., Steele, L.P., Strode, S.A., Sudo, K., Szopa, S., van der Werf, G.R., Voulgarakis, A., van Weele, M., Weiss, R.F., Williams, J.E., Zeng, G., 2013. Three decades of global methane sources and sinks. Nat. Geosci. 6, 813–823.
- Kljun, N., Calanca, P., Rotach, M.W., Schmid, H.P., 2015. A simple two-dimensional parameterisation for Flux Footprint Prediction (FFP). Geosci. Model Dev. 8, 3695–3713.
- Kroon, P.S., Hensen, A., Van Den Bulk, W.C.M., Jongejan, P.A.C., Vermeulen, A.T., 2008. The importance of reducing the systematic error due to non-linearity in N<sub>2</sub>O flux measurements by static chambers. Nutr. Cycl. Agroecosystems 82 (2), 175–186.
- Kroon, P.S., Schrier-Uijl, A.P., Hensen, A., Veenendaal, E.M., Jonker, H.J.J., 2010. Annual balances of  $CH_4$  and  $N_2O$  from a managed fen meadow using eddy covariance flux measurements. Eur. J. Soil Sci. 61 (5), 773–784.
- Lassey, K.R., 2007. Livestock methane emission: From the individual grazing animal through national inventories to the global methane cycle. Agric. For. Meteorol. 142, 120–132.
- Laubach, J., Barthel, M., Fraser, A., Hunt, J.E., Griffith, D.W.T., 2015. Combining two complementary micrometeorological methods to measure CH<sub>4</sub> and N<sub>2</sub>O fluxes over pasture. Biogeosciences 13 (4), 1309–1327.

- Leytem, A.B., Dungan, R.S., Bjorneberg, D.L., Koehn, A.C., 2011. Emissions of ammonia, methane, carbon dioxide, and nitrous oxide from dairy cattle housing and manure management systems. J. Environ. Qual. 40 (5), 1383–1394.
- Liang, L.L., Campbell, D.I., Wall, A.M., Schipper, L.A., 2018. Nitrous oxide fluxes determined by continuous eddy covariance measurements from intensively grazed pastures: temporal patterns and environmental controls. Agric. Ecosyst. Environ. 268, 171–180.
- Lopez, M., Schmidt, M., Yver, C., Messager, C., Worthy, D., Kazan, V., Ramonet, M., Bousquet, P., Ciais, P., 2012. Seasonal variation of  $N_2O$  emissions in France inferred from atmospheric  $N_2O$  and  $^{222}\mbox{Rn}$  measurements. J. Geophys. Res. Atmos. 117 (D14), 1–12.
- Mathieu, N., Strachan, I.B., Leclerc, M.Y., Karipot, A., Pattey, E., 2005. Role of low-level jets and boundary-layer properties on the NBL budget technique. Agric. For. Meteorol. 135 (1–4), 35–43.
- Mathot, M., Decruyenaere, V., Stilmant, D., Lambert, R., 2012. Effect of cattle diet and manure storage conditions on carbon dioxide, methane and nitrous oxide emissions from tie-stall barns and stored solid manure. Agric. Ecosyst. Environ. 148, 134–144.
- Merbold, L., Eugster, W., Stieger, J., Zahniser, M., Nelson, D., Buchmann, N., 2014. Greenhouse gas budget (CO<sub>2</sub>, CH<sub>4</sub> and N<sub>2</sub>O) of intensively managed grassland following restoration. Glob. Chang. Biol. 20 (6), 1913–1928.
- Meredith, L.K., Commane, R., Munger, J.W., Dunn, A., Tang, J., Wofsy, S.C., Prinn, R.G., 2014. Ecosystem fluxes of hydrogen: a comparison of flux-gradient methods. Atmos. Meas. Tech. 7 (9), 2787–2805.
- Mishurov, M., Kiely, G., 2010. Nitrous oxide flux dynamics of grassland undergoing afforestation. Agric. Ecosyst. Environ. 139 (1–2), 59–65.
- Myhre, G., Shindell, D., Bréon, F.-M., Collins, W., Fuglestvedl, J., Huang, J., Koch, D., Lamarque, J.-F., Lee, D., Mendoza, B., Nakajima, T., Robock, A., Stephens, G., Takemura, T., Zhang, H., 2013. Anthropogenic and natural radiative forcing. climate change 2013: the physical science basis. In: Contribution of Working Group I to the Fifth Assessment Report of the Intergovernmental Panel on Climate Change.
- Pattey, E., Strachan, I.B., Desjardins, R.L., Edwards, G.C., Dow, D., MacPherson, J.I., 2006. Application of a tunable diode laser to the measurement of CH4 and N2O fluxes from field to landscape scale using several micrometeorological techniques. Agric. For. Meteorol. 136, 222–236.
- Pattey, E., Strachan, I.B., Desjardins, R.L., Massheder, J., 2002. Measuring nighttime CO<sub>2</sub> flux over terrestrial ecosystems using eddy covariance and nocturnal boundary layer methods. Agric. For. Meteorol. 113 (1–4), 145–158.
- Peltola, O., Hensen, A., Belelli Marchesini, L., Helfter, C., Bosveld, F.C., van den Bulk, W. C.M., Haapanala, S., van Huissteden, J., Laurila, T., Lindroth, A., Nemitz, E., Röckmann, T., Vermeulen, A.T., Mammarella, I., 2015. Studying the spatial variability of methane flux with five eddy covariance towers of varying height. Agric. For. Meteorol. 214, 456–472.
- Phillips, F.A., Leuning, R., Baigent, R., Kelly, K.B., Denmead, O.T., 2007. Nitrous oxide flux measurements from an intensively managed irrigated pasture using micrometeorological techniques. Agric. For. Meteorol. 143 (1–2), 92–105.
- Röckmann, T., Eyer, S., van der Veen, C., Popa, M.E., Tuzson, B., Monteil, G.,
  Houweling, S., Harris, E., Brunner, D., Fischer, H., Zazzeri, G., Lowry, D., Nisbet, E.
  G., Brand, W.A., Necki, J.M., Emmenegger, L., Mohn, J., 2016. In situ observations of the isotopic composition of methane at the Cabauw tall tower site. Atmos. Chem.
  Phys. 16 (16) 10469-10487
- Ruyssenaars, P.G., Coenen, P.W.H.G., Rienstra, J.D., Zijlema, P.J., Arets, E.J.J.M., Baas, K., Dröge, R., Geilenkirchen, G., t Hoen, M., Honig, E., van Huet, B., 2021. Greenhouse gas emissions in the Netherlands 1990-2019, National Institute for Public Health and the Environment (RIVM).
- Satar, E., Berhanu, T.A., Brunner, D., Henne, S., Leuenberger, M., 2016. Continuous  $CO_2$ /  $CH_4$ /CO measurements (2012-2014) at Beromunster tall tower station in Switzerland. Biogeosciences 13 (9), 2623–2635.
- Saunois, M., Stavert, A.R., Poulter, B., Bousquet, P., Canadell, J.G., Jackson, R.B., Raymond, P.A., Dlugokencky, E.J., Houweling, S., Patra, P.K., Ciais, P., Arora, V.K., Bastviken, D., Bergamaschi, P., Blake, D.R., Brailsford, G., Bruhwiler, L., Carlson, K. M., Carrol, M., Castaldi, S., Chandra, N., Crevoisier, C., Crill, P.M., Covey, K., Curry, C.L., Etiope, G., Frankenberg, C., Gedney, N., Hegglin, M.I., Höglund-Isaksson, L., Hugelius, G., Ishizawa, M., Ito, A., Janssens-Maenhout, G., Jensen, K.M., Joos, F., Kleinen, T., Krummel, P.B., Langenfelds, R.L., Laruelle, G.G., Liu, L., Machida, T., Maksyutov, S., McDonald, K.C., McNorton, J., Miller, P.A., Melton, J.R., Morino, I., Müller, J., Murguia-Flores, F., Naik, V., Niwa, Y., Noce, S., O'Doherty, S., Parker, R.J., Peng, C., Peng, S., Peters, G.P., Prigent, C., Prinn, R., Ramonet, M., Regnier, P., Riley, W.J., Rosentreter, J.A., Segers, A., Simpson, I.J., Shi, H., Smith, S. J., Steele, L.P., Thornton, B.F., Tian, H., Tohjima, Y., Tubiello, F.N., Tsuruta, A., Viovy, N., Voulgarakis, A., Weber, T.S., van Weele, M., van der Werf, G.R., Weiss, R. F., Worthy, D., Wunch, D., Yin, Y., Yoshida, Y., Zhang, W., Zhang, Z., Zhao, Y., Zheng, B., Zhu, Qing, Zhu, Qiuan, Zhuang, Q., 2020. The global methane budget 2000-2017. Earth Syst. Sci. Data 12 (3), 1561-1623.
- Schmidt, M., Glatzel-mattheier, H., Sartorius, H., Worthy, D.E., Levin, I., Forest, B., 2001. Western European N<sub>2</sub>O emissions: a top-down approach based on atmospheric observations. J. Geophys. Res. Atmos. 106 (D6), 5507–5516.
- Schwingshackl, C., 2013. Master Thesis. Institut für Umweltphysik, Heidelberg University, Heidelberg, Germany, p. 100.
- Schrier-Uijl, A.P., Kroon, P.S., Hensen, A., Leffelaar, P.A., Berendse, F., Veenendaal, E.M., 2010. Comparison of chamber and eddy covariance-based CO<sub>2</sub> and CH<sub>4</sub> emission estimates in a heterogeneous grass ecosystem on peat. Agric. For. Meteorol. 150 (6), 825–831.
- Solazzo, E., Crippa, M., Guizzardi, D., Muntean, M., Choulga, M., Janssens-Maenhout, G., 2021. Uncertainties in the emissions database for global atmospheric research (EDGAR) emission inventory of greenhouse gases. Atmos. Chem. Phys. 21, 5655–5683.

- Szegvary, T., Conen, F., Ciais, P., 2009. European 222Rn inventory for applied atmospheric studies. Atmos. Environ. 43 (8), 1536–1539.
- Tian, H., Xu, R., Canadell, J.G., Thompson, R.L., Winiwarter, W., Suntharalingam, P., Davidson, E.A., Ciais, P., Jackson, R.B., Janssens-Maenhout, G., Prather, M.J., Regnier, P., Pan, N., Pan, S., Peters, G.P., Shi, H., Tubiello, F.N., Zaehle, S., Zhou, F., Arneth, A., Battaglia, G., Berthet, S., Bopp, L., Bouwman, A.F., Buitenhuis, E.T., Chang, J., Chipperfield, M.P., Dangal, S.R.S., Dlugokencky, E., Elkins, J.W., Eyre, B. D., Fu, B., Hall, B., Ito, A., Joos, F., Krummel, P.B., Landolfi, A., Laruelle, G.G., Lauerwald, R., Li, W., Lienert, S., Maavara, T., MacLeod, M., Millet, D.B., Olin, S., Patra, P.K., Prinn, R.G., Raymond, P.A., Ruiz, D.J., van der Werf, G.R., Vuichard, N., Wang, J., Weiss, R.F., Wells, K.C., Wilson, C., Yang, J., Yao, Y., 2020.
  A comprehensive quantification of global nitrous oxide sources and sinks. Nature 586 (7828), 248–256.
- Ulyatt, M.J., Lassey, K.R., Shelton, I.D., Walker, C.F., 2002. Seasonal variation in methane emission from dairy cows and breeding ewes grazing ryegrass/white clover pasture in New Zealand. New Zeal. J. Agric. Res. 45, 217–226.
- Van Der Laan, S., Neubert, R.E.M., Meijer, H.A.J., 2009. Methane and nitrous oxide emissions in The Netherlands: ambient measurements support the national inventories. Atmos. Chem. Phys. 9 (24), 9369–9379.
- Van der Maas, C.W.M., Baas, K., Van den Born, G.J., Geilenkirchen, G., Te Molder, R., Nijdam, D.S., Peek, C.J., Van der Sluis, S.M., Coenen, P.W.H.G., Zijlema, P.J., Van den Berghe, G., 2010. Greenhouse gas emissions in the Netherlands 1990-2008 National Inventory Report 2010.
- Veer, G., 2006. Geochemical soil survey of the Netherlands. Atlas of Major and Trace Elements in Topsoil and Parent Material; Assessment of Natural and Anthropegenic Enrichment Factors. Utrecht University.

- Velthof, G.L., Brader, A.B., Oenema, O., 1996. Seasonal variations in nitrous oxide losses from managed grasslands in the Netherlands. Plant Soil 181 (2), 263–274.
- Velthof, G.L., Oenema, O., 1995. Nitrous oxide fluxes from grassland in the Netherlands: effects of soil type, nitrogen fertilizer application and grazing. Eur. J. Soil Sci. 46 (4), 541–549.
- Vermeulen, A.T., Hensen, A., Popa, M.E., Van Den Bulk, W.C.M., Jongejan, P.A.C., 2011. Greenhouse gas observations from Cabauw Tall Tower (1992-2010). Atmos. Meas. Tech. 4 (3), 617–644.
- Waldo, S., Russell, E.S., Kostyanovsky, K., Pressley, S.N., O'Keeffe, P.T., Huggins, D.R., Stöckle, C.O., Pan, W.L., Lamb, B.K., 2019. N<sub>2</sub>O emissions from two agroecosystems: high spatial variability and long pulses observed using static chambers and the flux-gradient technique. J. Geophys. Res. Biogeosci. 124 (7), 1887–1904.
- Winderlich, J., Gerbig, C., Kolle, O., Heimann, M., 2014. Inferences from CO<sub>2</sub> and CH<sub>4</sub> concentration profiles at the Zotino Tall Tower Observatory (ZOTTO) on regional summertime ecosystem fluxes. Biogeosciences 11 (7), 2055–2068.
- Wu, Y.F., Whitaker, J., Toet, S., Bradley, A., Davies, C.A., McNamara, N.P., 2021. Diurnal variability in soil nitrous oxide emissions is a widespread phenomenon. Glob Chang Biol 27 (20), 4950–4966.
- Yacovitch, T.I., Neininger, B., Herndon, S.C., van der Gon, H.D., Jonkers, S., Hulskotte, J., Roscioli, J.R., Zavala-Araiza, D., 2018. Methane emissions in the Netherlands: the Groningen field. Elem. Sci. Anthr. 6.
- Zahorowski, W., Chambers, S.D., Henderson-Sellers, A., 2004. Ground based radon-222 observations and their application to atmospheric studies. J. Environ. Radioact. 76 (1–2), 3–33.